Evaluation der Wertigkeit der Fluoreszenzlaparoskopie beim kindlichen Rhabdomyosarkom

Inaugural-Dissertation

zur Erlangung des Doktorgrades

der Medizin

der Medizinischen Fakultät

der Eberhard Karls Universität

zu Tübingen

vorgelegt von

Ioan Cristian Urla

aus

Bukarest, Rumänien

2014

Dekan: Professor Dr. I. B. Autenrieth

1. Berichterstatter: Professor Dr. G. Seitz

2. Berichterstatter: Professor Dr. S. Beckert

Contents

INTRODUCTION

Rhabdomyosarcoma (*rhabdos*, "rod", *mys* , "muscle", *sarkos*, "flesh") is a primary solid malignant tumor in children and adolescents that arises from the embryonic mesenchyme with the potential to differentiate into skeletal muscle (1). Because of its mesenchymal origin, it can arise in tissue that does not normally contain skeletal muscle (urinary bladder, bile ducts) (2).

The incidence of pediatric soft tissue sarcoma (STS) in Germany is 1:100 000 children (3). Comprising over 50% of all soft tissue sarcoma (STS) in children, rhabdomyosarcoma (RMS) is the most common soft tissue sarcoma (0.5:100 000 in patients < 15 years) and the third most common extracranial solid tumor in children after neuroblastoma and Wilms tumor, accounting for approximately 5% of all pediatric cancers (1, 4, 5). Boys and girls seem to be equally affected by RMS (sex ratio 1.1:1 boys vs. girls) with a peak incidence in early childhood. The median age at diagnosis is approximately 5 years (6).

Classification

The classification of RMS is based on histological criteria and is of critical importance regarding the prognosis of patients. Mainly, there are two subtypes: embryonal and alveolar (7, 8).

A**lveolar RMS (RMA)** occurs in approximately 20% of all cases and, due to its high predilection of spread to regional lymph nodes, it is commonly associated with a poor prognosis (9). Genetically, RMA is consistently associated with two reciprocal translocations. The most common of them (55%) t(2;13)(q35;q14) fuses the DNA binding domain of PAX3 with the regulatory domain of FKHR (FOXO1) and occurs more frequently in older patients, who have a worse outcome (10). The other variant t(1;13)(p36;q14) fuses the PAX7 gene with FKHR(FOXO1) and occurs more often in infants, who have a better prognosis (11). The result of these

translocations is an increase of PAX activity leading to the de-differentiation and proliferation of myogenic cells.

However, 20-25% of RMA lack these translocations (4, 12, 13). They represent a heterogenous group of tumors with alternate fusions, fusions without production of detectable RNA, tumors with only rare fusion-positive cells and those with no molecular evidence of fusion. The latter category constitutes the bulk of this group (14-16).

Williamson et al analyzed the fusion gene status of 210 RMS specimens, dividing them into three groups: RME, RMA fusion gene positive (RMAp) and RMA fusion gene negative (RMAn). Through analysis of clinical data and genomic profiling they were able to demonstrate that RMAn is practically indistinguishable from RME in terms of clinical presentation, outcome and molecular biology. Moreover, using array based comparative genomic hybridization (aCGH), they showed that the frequency of many specific amplifications and gains is significantly different in RMAp compared to RMAn and RME. For example, MYCN amplification was found to be present in 20% of all RMAp patients, in 4% of RME and in none of the RMAn. Additionally, aCGH analysis showed that gain of chromosome 8 occurred in 74% of RME samples, 55% of RMAn samples and none of RMAp samples (17).

These data support previous studies by Wachtel and Davicioni. Wachtel et al reported the consistent high expression of AP2ß and P-cadherin protein in RMAp specimens and endothelial growth factor receptor (EGFR) and fibrillin-2 in RME, while RMAn was shown to lack the expression of AP2ß and P-cadherin and to have levels of EGFR and fibrillin-2 intermediate between those of RMAp and RME (18). Davicioni et al did not show any signature distinguishing RMAn tumors from RME in their expression and loss of heterogeneity analysis (13).
Despite consensus among the authors of the above mentioned studies, there is an ongoing debate about how or as to even if molecular biology should be integrated

into the existing risk protocols (19-21). The integration of molecular biology into the risk stratification systems may result in a more precise classification of the patients and a better tailoring of the therapeutic regimen without compromising their survival.

The **embryonal RMS (RME)** occurs in approximately 65-70% of the cases. These patients have a better prognosis compared with those suffering from RMA. RME rarely spreads to regional lymph nodes. Genetically, no consistent molecular markers have been associated with RME, although there is a loss of heterozygosity (LOH) at the 11p15 in up to 80% of the cases (22). The LOH at this site has also been observed to induce an increased expression of IGF II, as the gene which encodes this factor lies also within this locus, thus possibly playing an important role in tumor growth (22).

Risk stratification

The risk stratification system has been developed to tailor the intensity of therapy to patient outcomes.

According to the CWS Guidance (Cooperative Weichteilsarkom Study) of the German Society of Pediatric Oncology and Hematology (Gesellschaft für Pädiatrische Onkoloige und Hämatologie – GPOH), the patients suffering from RMS are divided in 8 subgroups (A-H) which are subsequently assigned to one of the 4 categories of risk: low, standard, high and very high, based on postsurgical stage (Table I), histology, localization of the tumor, lymph node status, tumor size and patient's age (Table 2). This system is based on the results obtained from the CWS-96 trials (23, 24).

The **low-risk group** is defined by favorable histology, IRS stage I, no lymph node involvement, patient's age < 10 years and tumor size < 5 cm. It represents a group of patients accounting for 6-8% of the whole population of children suffering from

RMS. Most of these patients suffer from localized paratesticular RMS and have an excellent outcome (6).

The **standard risk group** is generally defined by favorable histology, IRS group I-III, no lymph node involvement, independent of patient's age and tumor size. The patients assigned to the *subgroup B* are similar to the ones from the low-risk group but have large tumors (>5cm) and are older than 10 years of age. In *subgroup C* are included the children with orbital, head and neck non-parameningeal RMS. To *subgroup D* are assigned the patients younger than 10 years of age having small tumors (< 5 cm) with favorable histology (RME) arising in the extremities, parameningeal sites and bladder-prostate (6).

In the **high-risk group,** patients > 10 years of age with tumors > 5 cm, unfavorable location but with favorable histology, IRS group II-III and no lymph node involvement are included. The patients with embryonal N1 tumors are also included in this group.

The patients with tumors of unfavorable histology, IRS group II-III and positive lymph nodes are considered at **very high-risk** of tumor recurrence (6).

IRS group	Definition
I	R0 resection of a localized primary tumor, without lymph node involvement
II	R1 resection of a localized primary tumor, with R0 or R1 resection of the involved lymph nodes
III	R2 resection of a localized primary tumor
IV	Distant metastases

Table 1. Postsurgical stage (IRS group) according to STSC (Soft Tissue Sarcoma Committee)

R0 resection: microscopically complete resection

R1 resection: macroscopically complete resection with microscopic residuals

R2 resection: macroscopic tumor rests

Risk group	Subgroup	Histology	IRS group (postsurgical stage)	Localization	Lymph node status	Tumor size	Patient's age
Low risk	A	Favorable	I	Any	N0	<5 cm	<10 years
Standard risk	B	Favorable	I	Any	N0	>5 cm	> 10 years
	C	Favorable	II, III	Favorable	N0	Any	Any
	D	Favorable	II, III	Unfavorable	N0	<5 cm	<10 years
High risk	E	Favorable	II, III	Unfavorable	N0	>5 cm	>10 years
	F	Favorable	II, III	Any	N1	Any	Any
	G	Unfavorable	I, II, III	Any	N0	Any	Any
Very high risk	H	Unfavorable	II, III	Any	N1	Any	Any

Histology	Favorable	RME
	Unvaforable	RMA
Localization	Favorable	Orbital (without infiltration of the bone) Head and neck-non parameningeal Urogenital-non bladder/prostate
	Unfavorable	Orbita with bone infiltration Head and neck-parameningeal Urogenital-bladder/prostate Extremities Others (thorax, pelvis, abdominal wall)
Lymph node status	N0	No involvement
	N1	Lymph nodes involved

Table 2. The risk stratification for RMS according to the CWS Guidance (6).

Treatment

The treatment of children suffering from RMS is multimodal and includes chemotherapy in conjunction with either surgery, radiation therapy or a combination of both, in order to maximize local tumor control.

In the CWS Guidance, which is used in Germany, Austria, Switzerland, Poland, and Sweden, the sequence and the intensity of the treatment depend on the stage, localization of the tumor, tumor size, histology, age at diagnosis and are adapted to the risk categories.

Chemotherapy

Chemotherapy regimen in the current CWS guidance are based on the results of the CWS-96 trial (Literatur) and depend on the specific risk group. In general, patients are treated with a multidrug chemotherapy regimen including alkalators, alkaloids, actinomycin-D as well as platin derivates. In most cases, chemotherapy is applied for 3 cycles prior to local control. Chemotherapy is continued after local therapy for several cycles depending on the risk stratification.

Radiotherapy

Radiotherapy is an essential treatment modality for selected cases of RMS. Generally, it is administered after 3 cycles of induction chemotherapy. IRS stage, lymph node status, histology and tumor response to chemotherapy after 9 weeks of treatment are essential for stratification of local control.

The following guidelines for RT have been proposed in the CWS guidance:
Patients with initial complete resection (R0), no lymph node involvement and favorable histology should not be irradiated, while those with alveolar histology should receive a dose of 41.4 Gy administered in 23 fractions (6).

These recommendations are based on the study by Wolden et al regarding the benefit of radiotherapy in patients with IRS Group I and from the IRS I-III trials (25). The authors showed that patients in the RMA post-surgical stage I benefit from radiotherapy (5-year OS 82% vs 52%) while patients with favorable histology do not (10-year OS 95% with or without radiotherapy).

Patients with grossly resected tumor but microscopic residual disease should receive 41.4 Gy in 23 fractions, regardless of histology (6). The recommendations are made in conformity with the study by Schuck et al. The authors, analyzing the benefit of radiotherapy in patients with RMS IRS Group II treated in the CWS trials 81-96, showed an improved survival in the patients who received radiotherapy (84% vs 77%). The improvement in local control (83% vs 65%) and EFS (76% vs 58%) was independent of histology, tumor size, tumor location and patient's age (26).

In patients with macroscopic residual disease and residual disease following initial chemotherapy, a secondary complete resection (R0, with tumor-free margins) prior to radiotherapy is recommended if feasible. Radiotherapy usually should follow secondary resection. If a complete secondary resection is not feasible after neoadjuvant chemotherapy but might be possible with further tumor shrinkage, radiotherapy should precede surgery (6).

The preferred mode of administration of radiotherapy is conventional fractionation, i.e. 1.8 Gy per day. In patients < 3 years of age or those with large abdominal fields, smaller fractions may be used. Brachytherapy may be used in cases of incompletely resected tumors of the vagina, perineum, bladder, prostate and orbit (6).

Prognosis

The prognosis of patients suffering from RMS depends on the age at diagnosis, localization of the tumor, histology, stage, clinical group and response to therapy (9). Patients assigned to the low-risk group have an excellent prognosis with 5-year event-free survival (EFS) and overall survival (OS) of 88% and 97% respectively (27). Patients with metastases at diagnosis (high-risk group) have the worst outcome with 5-year EFS and OS rates of 57% and 67%, respectively (27). Patients assigned to the standard-risk group have a 5-year EFS and OS of 72% and 95%, respectively. However, the prognosis of these tumors is poor, the 5-year EFS and OS rate independent of stage being 67% and 78%, respectively (28).

The role of the surgery in the treatment of children suffering from RMS

Surgery plays a key role in the treatment of children suffering from RMS as complete tumor resection is one of the main prognostic factors preventing local tumor recurrence (29). Completely resected tumors at the time of primary diagnosis present a lower risk of relapse and have a better post-relapse prognosis as reported by Dantonello et al (24). Even in patients with relapsed RMS, the removal of the tumor by a second-look operation seems to be essential to maintaining a stable remission (30).

The main problem in the surgery of these tumors is the lack of a clear delimitation between the tumor and healthy tissue, especially in complex anatomical regions such the bladder, the prostate, the pelvis, and the porta hepatis. Therefore, mutilating surgery is sometimes necessary to acquire a complete resection in order to prevent local recurrence.

Radiotherapy as an integral part of local control will be needed in selected cases. It might help to reduce tumor volumes, thus avoiding radical surgical procedures.

Therefore, the timing of radiotherapy has to be coordinated with surgery. However, the side effects of radiotherapy such as breast aplasia, impairment of respiratory function, potentiation of the cardiotoxic effect of actinomycin-D and adriamycin) as well as secondary malignancies should be considered (31).

Identification of tumor margins is even more difficult in cases of tumor relapse. In these patients, the interpretation of imaging studies is difficult due to a poor discrimination between tumor tissue and scarring. Under these circumstances, novel diagnostic and therapeutic modalities aimed to improve the intra-operative visualization of the tumors and their margins are required. One such option is fluorescence diagnosis also known as photodynamic diagnosis (PDD) and photodynamic therapy (PDT).

The role of photodynamic diagnosis (PDD) in the improvement of the intraoperative detection of the tumors

The principle of photodynamic diagnosis (PDD) is to enhance the contrast between the tumor and healthy tissue by the interaction of the light of a specific wavelength with a photosensitive agent, which ideally should have a great affinity to cancer cells (32). This method has received significant interest in surgical oncology improving the early detection of breast, urogenital, pulmonary, and gastrointestinal cancers (33-37).

In pediatric solid tumors, there are only very limited reports on PDD. Videoscopic fluorescent diagnosis of peritoneal and thoracic metastases using 5-aminolevulinic acid (5-ALA) was reported in a rat model of human hepatoblastoma (38). Our group has previously demonstrated that *in vivo* visualization of xenotransplanted pediatric RMS after transfection with red fluorescent protein is effective (39). Additionally, we could demonstrate *in vivo* cancer cell trafficking of RMS cells and describe different mechanisms of metastatic invasion using this technique (15).

The potential clinical utility of fluorescent proteins in RMS is limited as they need to be bound to specific antibodies. The problem in RMS is the absence of specific cell surface receptors. However, Hermann et al analysed the expression of cell surface EGFR (epidermal growth factor receptor) on 3 RMS cell lines by flow cytometry and demonstrated that ERMS and ARMS exhibited a high expression of EGFR (40). Therefore, EGFR may function as a target for therapeutic antibodies. Cetuximab is a monoclonal antibody that targets the extracellular domain of EGFR. Thus, the labeling of this antibody with a fluorochrome may lead to the specific detection of the tumor based on its fluorescence. Withrow et al. successfully demonstrated *in vivo* visualization of tumor cells using cetuximab conjugated with indocyanine green (ICG) in a mouse model of head and neck cancer (41).

ALA is an intermediate in hem biosynthesis in the body. In the biosynthetic pathway of heme, ALA is converted into protoporphyrin IX (PpIX), an endogenous fluorescent photosensitizer, which selectively accumulates in tumor cells due to changes in the activity of two enzymes: prophobilinogen deaminase (increased activity) and ferrochelatase (decreased activity) as shown in the **Figure 1.** When excited by blue light, Pp IX generates red fluorescence (33, 42). 5-ALA derived Pp IX fluorescence has been successfully used for intraoperative visualization of malignant gliomas, improving the prognosis of patients (43). Moreover, a long-sustaining response (56 months) in a patient with non-resectable reccurence of a glioblastoma multiforme after treatment with interstitial photodynamic therapy (iPDT) was reported (44). However, this photosensitizer is rapidly bleached out and exposure to light is limited to short illumination periods (32).
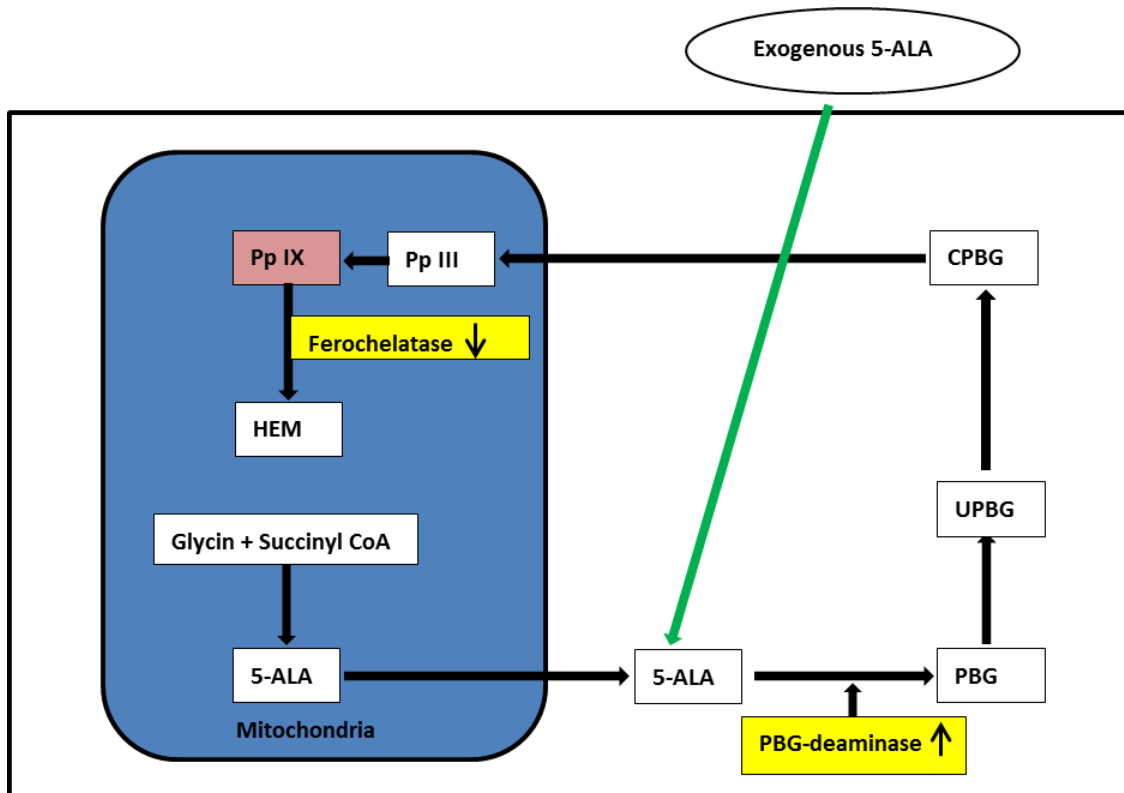
Figure 1. Heme biosynthetic pathway and 5-ALA metabolism into Pp IX

Pp IX: protoporphyrin IX; Pp III: protoporphyrin III; PBG: porphobilinogen; UPBG: uroporphobilinogen; CPBG: coproporphobilinogen;

Hypericin is a hydroxylated phenanthroperylenequinone derivate, isolated from plants of St. John´s Wort *(Hypericum perforatum),* a naturally occurring herb in Europe and Asia. It has primarily been used for the treatment of depressive disorders (45), but in recent years has been described for *in vivo* visualization of bladder cancer (46). Selective accumulation of hypericin in tumor cells was reported by several authors (47-50). Hypericin has a great photostability and a lower fluorescence clearance in comparison to ALA, (46). Comparing the cellular uptake and photodynamic inactivation of meduloblastoma cells *in vitro*, after incubation with hypericin and 5-ALA, Ritz *et al* convincingly demonstrated that the fluorescence and phototoxicity of hypericin are superior to those determined by 5-

ALA: 5-fold increase in fluorescence and 8-13 fold lower LD_{50} (Light Dose $_{50}$: the light dose that is required to reduce cell survival to 50% of control) (51).

Photodynamic therapy (PDT), currently studied as a novel treatment approach in various malignancies, involves the systemic or topical administration of a photosensitizer followed by exposure of the tumor with light of appropriate wavelength. In the presence of oxygen, photoactivated sensitizers generate highly reactive oxygen species (ROS). The oxidative damage to various cellular organelles and functions induced by ROS leads to direct cytotoxicity on tumor cells (52). Beside its fluorescending properties, hypericin is also a very potent photodynamic agent and after activation with light of appropriate wave length (excitation 590 nm, emission 640 nm), it produces singlet oxygen efficiently (quantum yield of 0.73) resulting in the apoptosis of the tumor cells (53, 54). We previously reported the successful *in vitro* photodynamic therapy of RMS cells (47) and pediatric epithelial liver tumors (55) promoted by hypericin, but the transfer of this data into an *in vivo* setting is difficult due to the necessity of a tumor selective accumulation of the photosensitizer in RMS. In children this is even more difficult due to the accelerated metabolism and rapidly growing tissue.

Up to now there is no data on *in vivo* photodynamic diagnosis and therapy using fluorescence laparoscopy in pediatric RMS.

Objectives of the study

The aim of this study was to investigate the feasibility of fluorescence laparoscopy using different photodynamic agents in a mouse model of disseminated pediatric RMS. Additionally, we wanted to figure out if hypericin-induced photodynamic therapy on childhood alveolar RMS cells might be feasible *in vivo* as a novel promising treatment option for advanced-stage RMS. For this purpose, we tried to answer the following questions:

1. It is possible to perform an *in vivo* detection of RMS tumors based on the expression of the mCherry reporter protein using fluorescence laparoscopy?
2. Is the *in vivo* detection of RMS tumors based on their vascularization using fluorescence laparoscopy, after i.v. injection of ICG, possible?
3. Is the *in vivo* specific detection of RMS tumors based on their surface antigen using fluorescent labeled Cetuximab in the setting of fluorescence laparoscopy feasible?
4. Is the detection of the RMS xenotransplants possible using hypericin-based fluorescence laparoscopy?
5. Is *in vivo* hypericin-induced photodynamic therapy possible during laparoscopy?
6. Is a therapeutic intervention in this system comprehensible?

MATERIALS AND METHODS

Cell lines and culture conditions

The alveolar RMS cell line Rh30 (DSMZ, Braunschweig, Germany) was used for this study. This cell line was obtained from a bone metastasis of a 17-year old young man suffering from an alveolar RMS.

All cells were cultured in DMEM medium (GIBCO, Berlin, Germany) supplemented with 10% fetal calf serum, 1% L-Glu, 2.5% HEPES and antibiotics (Penicillin/Streptomycin, Biochrom, Berlin) in a humidified atmosphere containing 10% carbon dioxide at 37°C. All cells were mycoplasma negative. The medium was changed every second day and the cells were passaged if a confluence rate of 80% was reached. These procedures were performed under sterile conditions in cabinets with laminar flow filtered air.

Medium change

The supernatant consisting of medium and nonviable cells was aspirated using a vacuum pump and Pasteur pipettes. Approximately 5 ml of warmed PBS solution (Biochrom, Berlin) was added and the Petri dishes were gently swirled to remove the cellular debris. Then the PBS solution was aspirated and 8 ml of fresh culture medium was added.

Passage of the cells

The supernatant was aspirated and the cells were washed with PBS previously warmed at 37°C. To detach the adherent cultures from the bottom of the plate, 2 ml of trypsin (PAA Laboratories, Pasching, Austria) was added. After 2 minutes, culture medium was added in order to inhibit the activity of trypsin and to stop the proteolysis. The cell suspension was aspirated and centrifuged for 5 minutes at 600 rotations /minute. After centrifugation, 4/5 of the cells were removed or divided into new Petri dishes. Five milliliters of fresh culture medium per Petri dish was added to the remaining cells.

Determination of the number of cells

For determination of the number of cells, 10 µl of the cell suspension were dropped laterally and aspirated by the capillary force into the Neubauer counting chamber (Roth, Karlsruhe, Germany). Under light microscopy (40X magnification) 4 great quadrants were counted. To determine the number of cells/ml, the cell number counted was divided by 4 and multiplied with the chamber factor 10^4. Based on the number of the cells/ml, the absolute number of cells could be determined in the cell suspension. Further, the cells were centrifuged for three minutes at 1300 rotations/minute, the supernatant aspirated and the desired cell concentration resuspended in culture medium.

Transduction of the Rh30 cell line with mCherry reporter protein (mCherryLentifect®)

The transduction of the Rh 30 cells in order to stably express the red fluorescent protein mCherry was carried out using the kit and the guidelines from GeneCopoeiaInc (mCherry Lentifect®, Rockville, U.S.A.). For the efficient expression of the red fluorescent protein mCherry, the lentiviral particle contains a CMV promoter and a puromycin cassette (**Figure 2**). The Rh30 cells were cultured in 24 well plates (Becton Dickinson, Heidelberg, Germany) until they reached 80% confluence. Polybren 6µg/ml (Gibco/Invitrogen, Darmstadt, Germany) was added in order to facilitate the penetration of the viruses into the cells. After application of 10µl mCherryLentifect®/plate the plates were incubated for 24 hours at room temperature. The following day the medium was changed and the lentivirus was chemically neutralized. For selection, 0.3µg/ml Puromycin® (Sigma-Aldrich, München) was added at every medium change until drug-resistant colonies became visible (56).
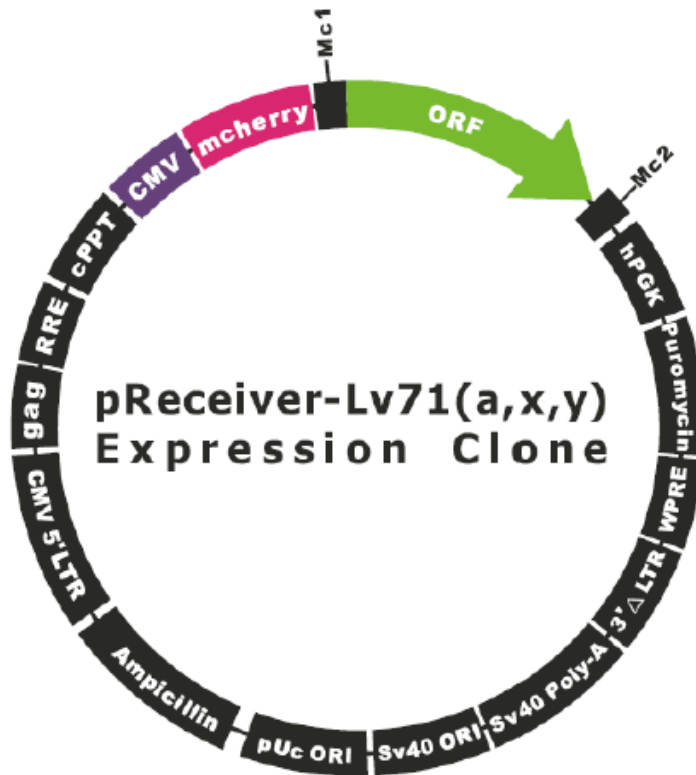
Figure 2. Schematic representation of the lentiviral transfer vector that expresses the mCherry protein (micrograph from the manufacturer)

Fluorochromes

mCherry is a monomeric red fluorescent protein derived from a protein isolated from *Discosoma sp.* It is used in biotechnology as a tracer to follow the flow of fluids as well as a marker when labeled to molecules or cell components. It matures rapidly allowing it to be visualized very soon after activating transcription. It has a peak absortion at 587 nm and emission at 610 nm (Table 4). It is highly photostable and resistant to photobleaching (57) (**Figure 3**). Due to its high photostability and low molecular weight it is considered the best general-purpose red monomer (58).
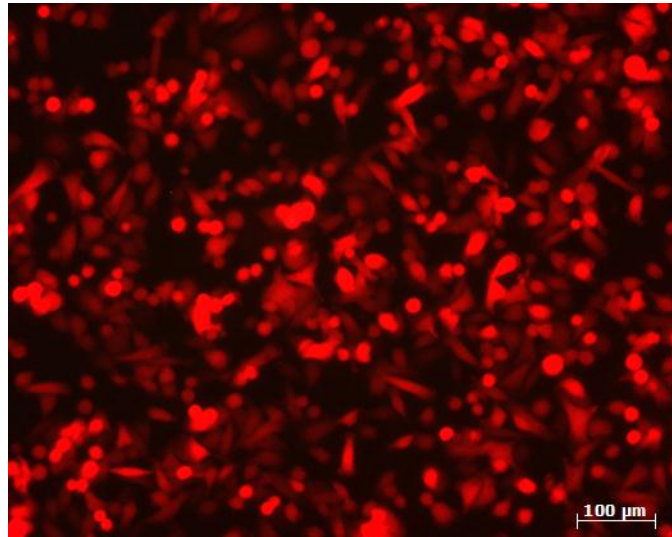
Figure 3. mCherry expressing tumor cells as seen by fluorescence microscopy

Indocyanine green (ICG) is a tricarbocyanine dye which is internationally approved for use in cardiac, (micro) circulatory and liver function diagnosis (59). It is an ideal agent for imaging vessels as it bounds tightly to plasma proteins and therefore remains strictly intravascular. The excitation (600-900 nm) and emission (750-950 nm) profiles of ICG are in the near infra-red (NIR) wavelengths, which allow light penetration and imaging of vessels below a few millimeters of tissue (60) (**Figure 4, Table 3**).
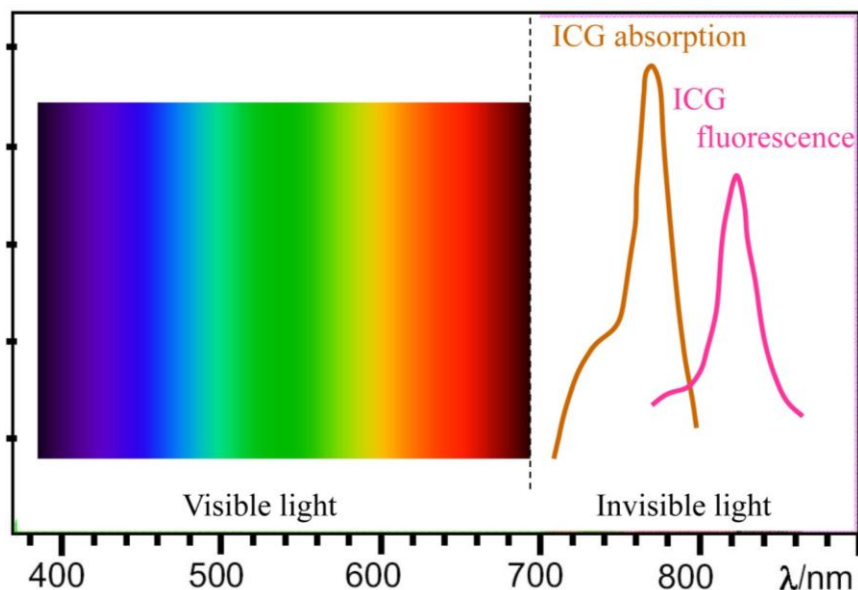
Figure 4. Maximal absorption and emission spectrum of ICG. Modified from (61).

Hypericin, a hydroxylated phenanthroperylenequinone derivate is a constituent of plants of the genus *Hypericum perforatum* (**Figure 5**) (54). Its affinity against tumor cells was demonstrated by several studies (47, 54, 55). After activation with light of appropriate wave length (excitation 590 nm, emission 640 nm), it produces singlet oxygen efficiently (quantum yield of 0.73) resulting in apoptosis of the tumor cells (53, 54). Hypericin is present as a constituent in *Hypericum* extract, which is clinically used as an antidepressant (45). In recent years it has been described for *in vivo* visualization of bladder cancer (62) and has been studied as a photodynamic agent in different tumor entities (63-68). The impressive anti-angiogenic effects of hyepericin were also reported by several authors (66, 68) (see **Table 3**)
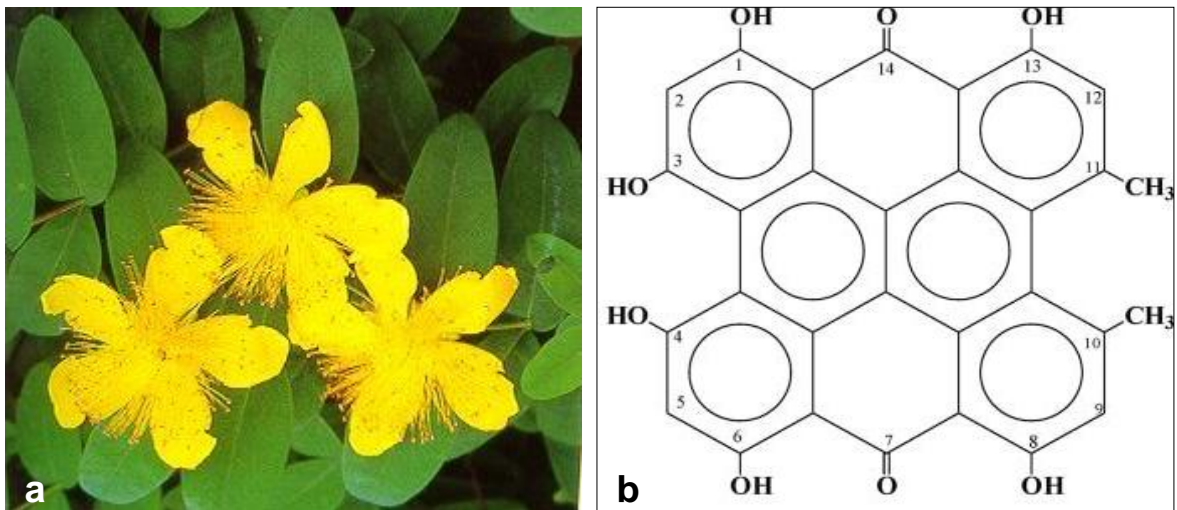
Figure 5. a. *Hypericum perforatum*, the herb from which hypericin is extracted **b.** Chemical structure of Hypericin. Modified from (54).

Photosensitizer	Maximal absorption	Maximal emission
mCherry (57)	587 nm	610 nm
ICG (69)	780 nm	820 nm
Hypericin (70)	590 nm	640 nm

Table 3. Maximal spectral absorption and emission of the photosensitizers used

Labeling of Cetuximab with ICG

Labeling of Cetuximab (Erbitux, Merck, Darmstadt, Germany) with ICG (DojindoEu GmbH, Munich, Germany) was performed as suggested by the manufacturer. To this purpose, the sample solution containing 200 µg Cetuximab (Erbitux, Merck, Darmstadt, Germany) was mixed with 100 µl WS Buffer, using a pipette, in a filtration tube. The solution obtained was centrifuged at 8000 rotations/minute for 15 minutes.

To prepare the ICG solution, 500 µl NH_2-Reactive ICG 10 µl DMSO was added into the NH_2-Reactive ICG tube and dissolved by pipetting. Reaction Buffer (100 µl) and NH_2-Reactive ICG solution (8 µl) were added in the filtration tube, mixed by pipetting and then incubated at 37°C for 10 minutes. After 10 minutes, 100 µl WS Buffer (DojindoEu GmbH, Munich, Germany) was added and the filtration tube was centrifuged at 8000 rotations for 15 minutes. After centrifugation, another 200µl WS Buffer was added and centrifugation at 8000 rotations per minute was performed for 15 minutes. The final step was to add 200 µl PBS to the product and pipette it 10 times to recover the conjugate. A final concentration of 200µg/200µl was obtained.

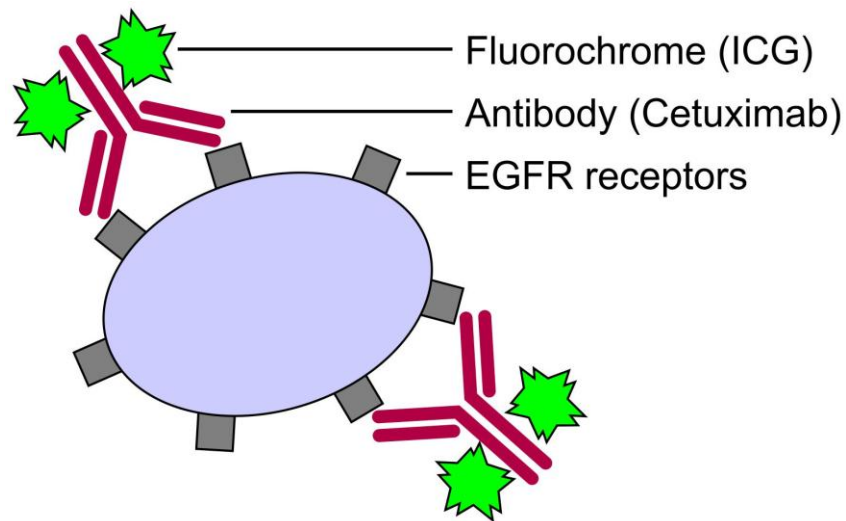**Figure 6.** Schematic representation of ICG-labeled Cetuximab

Labeling efficiency was estimated using flow cytometry and the Odissey system (LI-COR Biosciences GmbH, Bad Homburg, Germany). The Odissey system is an imaging system, which uses infrared laser excitation resulting in decreased excitation light leakage, higher signal-to-noise ratio and sensitive detection of low abundant targets (proteins, antibodies, etc.).

To this purpose, Rh30 cells were incubated with labeled antibody at 0.1 to 5µg/ml and visualized in flow cytometry with the LSR II (BD, Heidelberg, Germany). Staining of adherent Rh30 cells with ICG conjugated Cetuximab was revealed by the Odissey system.

Animal model

NOD/LtSz-scid IL2Rγnull-mice were used for this study. This mouse strain was initially described by Schultz et al. (71). These animals have severe impairments in innate immunity due to the absence of the IL2Rγ gene. This gene is responsible for encoding the γ chain of the interleukin-2 receptor (IL2R) and plays an important role in growth and differentiation of T-cells, B-cells, NK-cells and monocytes.

The animals were kept in pathogen-free conditions, on an autoclaved standard diet and given free access to sterilized water.

Xenotransplantation of the tumor cells

Tumor induction was carried out using human alveolar RMS cells (Rh 30) in all the experiments. For xenotransplantation, the tumor cells were trypsinized as previously described. The cells were washed with PBS, centrifuged and then resuspended in 200 µl DMEM. A total number of 2×10^6 RMS cells were injected intraperitoneally in every mouse.

After xenotransplantation, the mice were clinically evaluated every day and the weight was measured. In case of a weight loss of more than 20%, combined with the loss of appetite, diarrhea and apathy, the animal was sacrificed.

Design of the animal experiments

All animal experiments were approved by the local government ethics committee for animal studies (Regierungspräsidium Tübingen, K5/11) and were performed under sterile conditions.

Seventeen NOD/LtSz-scidIL2Rγnull-mice were used. In order to analyze different photosensitizers, the mice population was divided into 4 groups as shown in **Table 4**.

Group	Fluorochrome	Objective	Dosage/mouse	n
1	mCherry	Tumor detection based on stable mCherry expression	Stable transduction	5
2	ICG	Tumor detection based on neovascularization	100µg/100 µl	3
3	ICG-cetuximab	Specific tumor detection based on EGFR	100µg/mouse	4
4	Hypericin	Tumor detection based on the hypericin-uptake of the tumor cells	100µg/200 µl	5

Table 4. Objectives of the examination and the dosages of the fluorochromes used

In the first group, tumor induction was carried out with genetically modified Rh 30 cells to stably express the red fluorescent protein mCherry after excitation with light of the appropriate wave length.

In the following three groups, tumor induction was carried out using non-transfected, non-fluorescending Rh 30 cells. The application of the fluorochromes was carried out in the following way:

In the second group, 100µg/µl indocyanine green (ICG) was injected intravenously at the time point of initiation of laparoscopy. The objective was to evaluate the detection of the tumor based on its vascularization. Photosensitisation times (time interval between application of photosensitizer and light excitation) of 5 minutes

were chosen based on the previous experience of other authors in other studies (59).

In the third group, in order to increase the specificity of the method, we evaluated the *in vivo* detection of the tumor cells based on its surface antigens (EGFR). We previously demonstrated that Cetuximab specifically binds to EGRF expressed by Rh 30 cells *in vitro* (40)*.* Therefore, 100μg of ICG-labeled Cetuximab was intravenously injected 24 hours prior to laparoscopy.

In the fourth group, we evaluated the detection of the tumors based on their hypericin uptake. Selective accumulation of hypericin in the tumor cells was previously reported by several authors (47, 54). The photosensitization was carried out using hypericin (Merck, Darmstadt, Germany) at a concentration of 100μg/200μl/mouse, intravenously injected 24 h prior to laparoscopy.

To evaluate the effects of photodynamic activation of hypericin on tumors and surrounding tissue during laparoscopy, the tumors located in the porta hepatis and on the greater curvature of the stomach underwent excitation with blue light for 5 minutes. The animals were kept for 4 hours in the dark to avoid photosensitivity and to allow the initiation of apoptosis. Tumors and livers were then collected and stored deep frozen to evaluate apoptosis by a terminal desoxyribosyl-transferase-mediated dUTP nick-end labeling test (TUNEL).

Fluorescence laparoscopy

Equipment

We used the Karl Storz D-Light System (Karl Storz GmbH&Co., Tuttlingen, Germany). Two models of this system are available, both capable of different illumination modes.

The D-Light P system has been tailored to meet the requirements of ICG fluorescence imaging. This system is equipped with an excitation light source (100W short-arc xenon lamp) and a specifically designed optical filter mounted on a filter wheel that can be activated using a button placed on the camera head. Using this button, the filter can be placed or removed, thus the excitation wavelength from the light source may be shifted from the conventional white light (WL mode) to blue light (AF mode: 380-450 nm) or near-infrared light (ICG mode: 690-780 nm). Additionally, a long pass filter, located in the eyepiece of the telescope allows the passage of 790 nm and longer, which corresponds to the emission wavelength of the fluorochromes used. We used this system in the first three groups for the detection of the mCherry and ICG-determined fluorescence.

The D-Light C system was created to improve the detection of different types of tumors based on their fluorescence after injection of a specific fluorescence agent and excitation with light of the appropriate wave length. This system is also equipped with a xenon 100 W short arc lamp with filter options for white light (WL mode) and fluorescence excitation (AF mode: 380-450 nm). The eyepiece of the telescope has integrated a long pass filter (> 520 nm) to block the reflected blue excitation light without blocking the red fluorescence. We used this system in the fourth group for the detection of hypericin-determined fluorescence.

For optimal transmission of the excitation light, the systems are provided with a special fluid light guide. A special modified camera (Tricam SL II, Karl StorzGmbH&Co., Tuttlingen, Germany) was used for documentation. The camera presents several features: enhanced sensitivity in the wavelength range greater than 600 nm, automatically and manually adjustable target integration of images in fluorescence mode, two independent white balances for white light and fluorescence and the possibility to switch the mode of illumination from the camera head (72).

Photosensitizer	System	Mode	Excitation	Emission
mCherry	D-Light P	AF	380-450 nm	610 nm
ICG/ICG-Cetux.		ICG	690-780 nm	LP 790 nm
Hypericin	D-Light C	AF	380-450 nm	LP > 520 nm

Table 5. Optical properties of the laparoscopic system

Procedure

Fluorescence laparoscopy was performed 3 weeks after tumor induction. All surgical procedures were performed under general anesthesia with Ketamin 10% and Xylazin 2%, 100µl/10g mouse injected intraperitoneally. After anesthesia, the mouse was placed in the supine position, on a heating plate. The abdominal hair was chemically removed using a depilatory creme (Veet, Mannheim, Germany). Under sterile conditions, a small incision was carried out in the lower middle abdomen for the placement of a 5-mm optical port. To maintain proper insufflation, a purse-string suture was placed around this incision. The insufflation was carried out with carbondioxide 0,5l/min flow and 2 mmHg pressure using a thermoflator (SCB Thermoflator, Karl StorzGmbH&Co., Tuttlingen, Germany). After insufflation, a 3-mm 0° laparoscope (Karl StorzGmbH&Co., Tuttlingen, Germany) was introduced in the abdominal cavity. The procedure started with the inspection of the abdominal cavity using white light. The tumors detected were counted and the location was noted (73).
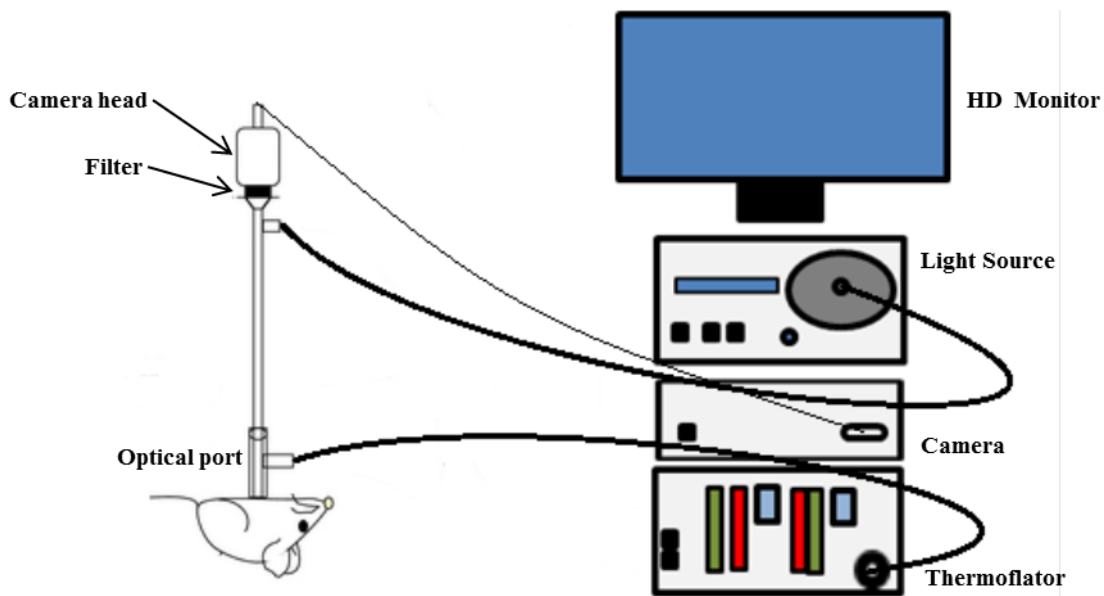
Figure 7. Schematic representation of laparoscopic system (Storz D-Light, Karl Storz GmbH&Co., Tuttlingen, Germany)

After laparoscopy, a laparotomy was performed and 3 tumors / mouse were resected using the fluorescence as guidance. After resection, the fluorescence of the tumor bed was documented and tumors together with the resection margins were histologically analyzed. At the end of the operation, the mice were sacrificed by administration of a lethal dose of anesthetics (73).
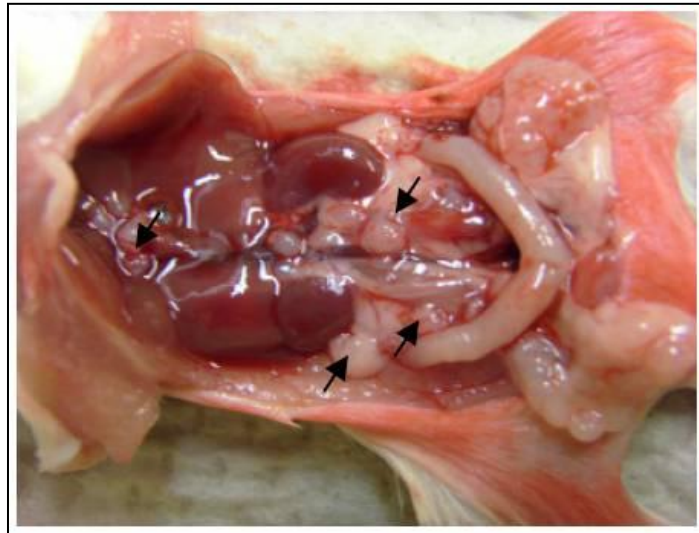
Figure 8. The abdominal cavity of the mouse, as seen during laparotomy. The arrows indicate the tumors

In vivo photodynamic therapy

For the evaluation of photodynamic therapy, only animals from the fourth group, in which the photosensitization was carried out with hypericin were suitable. In these mice, after laparoscopy, the tumors located on the lesser curvature of the stomach and in the porta hepatis were exposed to blue light (AF mode of the D-Light C system, Karl StorzGmbH&Co., Tuttlingen, Germany) for 5 minutes. The abdominal wound was closed and the mice were kept in a dark environment to avoid photosensitivity. After 4 hours, a laparotomy was performed and the tumors as mentioned previously were collected and stored in liquid nitrogen. To verify possibly induced apoptosis in the surrounding tissue inadvertently exposed to blue light during the procedure, the livers of the mice were collected and analyzed together with the tumors. To evaluate apoptosis induced by the photoactivation of hypericin, a terminal desoxyribosyl-transferase-mediated dUTP nick-end labeling test (TUNEL) was performed (73).

Evaluation of apoptosis after photodynamic therapy - TUNEL test

For investigation of induced apoptosis in tumors and surrounding tissues Terminal deoxyribosyl-transferase-mediated dUTP nick-end labeling test (TUNEL) was performed. Therefore, 10 µm cryosections of the tissue involved were rinsed in PBS. The cells were fixed with Roth-Histofix solution (Roth, Munich, Germany) and rinsed in PBS three times. Slides were then incubated in 0.1% Triton/PBS (Merck, Darmstadt, Germany) on ice for 2 minutes and rinsed with PBS. For positive controls, cells were incubated with DNase I (Roche Diagnostics) 1:10 in PBS, 15 minutes at room temperature. TUNEL reaction solution (50µl/well, Roche Diagnostics, #1684795, Pinzberg, Germany) was added for 60 minutes at 37°C. For negative controls, 50µl/well of labeling solution without enzyme (Roche Diagnostics, #1684795) was added. Slides were rinsed in PBS for three times. For nuclear counterstaining, DAPI was used for 1 minute (Sigma-Aldrich, #D-9452, Munich, Germany, dilution 1:10 000), followed by washing in PBS three times, each time for 5 minutes**.** The slides were then mounted with mounting medium (Dako, Glostrup, Denmark) and analyzed by fluorescence microscopy (Zeiss AxioVision, Carl Zeiss Microscopy GmbH, Germany)(73).

Histological analysis

Paraffin embedding and paraffin sections

To preserve tissue morphology, the specimens obtained during the surgery were fixed in 3.7% formalin for 24 hours. Tissues were dehydrated using ascending ethanol series (70%, 90% and 100% ethanol) and xylole (Xylol$^®$, Merck, Darmstadt, Germany) for 60 minutes. After dehydration, the tissue was embedded in paraffin using the automated tissue processing system from the Department of Pathology of the University Hospital Tübingen and the paraffin blocks obtained were stored at room temperature.

To obtain thin paraffin sections, the block was previously cooled for 24 hours at -20°C. Thin sections (3 µm) were performed using a microtome. The slices obtained were placed in a water bath at 45°C using a wet brush. The paraffin section was then positioned on the glass slide, transferred to a warm drying platform and dried at 60°C.

Hematoxylin-eosin staining

The paraffin sections obtained as previously described were deparaffinized using ethanol and xylole. After deparaffinization, the slides were stained with Mayer hematoxylin solution (Merck, Darmstadt, Germany) for 2 minutes and then washed with running tap water for 5 minutes. For counterstaining, the slides were bathed in eosin solution for 1 minute, then dehydrated using ethanol ascending series and mounted with a xylole-based medium. For histological evaluation, 10 high power fields per slide were used.

Data processing

The images obtained during laparoscopy were not processed in any way. Representative frames are presented. The histologic images were processed for brightness and contrast using the AxioVision (Carl Zeiss Microscopy GmbH, Germany) digital image processing software.

Statistics

Descriptive statistics for continuous variables are expressed as median and range. Significance was assumed for all results with $p < 0.05$.

RESULTS

Initially, 25 NOD/LtSz-scid IL2Rγnull mice were used for this study. Three weeks after tumor induction, tumor growth was observed in 22 mice. In three mice no tumor growth occurred. Five mice died due to tumor progression. The remaining 17 mice represent the population used further in the study. This population was divided into 4 groups in order to investigate different photosensitizers.

Group I – Detection of RMS tumors based on the expression of the mCherry reporter protein using fluorescence laparoscopy (n=5)

The conventional laparoscopy (WL mode) revealed a total number of 32 tumors in all 5 animals (median 6 tumors/mouse [2-10]). Among these, 13 suspicious lesions (median 3 tumors/mouse [1-4]) were not fluorescending after excitation with blue light (AF mode) and were considered false positive. The histological examination of these structures revealed no RMS cells. The remaining 19 tumors in all 5 animals (median of 3 tumors /mouse [1-7]) were visible under both conventional (WL mode) and blue light (AF mode) as red fluorescending tissue. These tumors had a median size of 4.8 mm [1.6 – 7.7] and were characterized by a prominent appearance as shown in the **Figure 9 a, b**.

Additional 38 tumors in all 5 animals (median per animal: 11 tumors [range 3-20] p=0.026), which were not visible during conventional laparoscopy due to their plane morphology and small dimensions (median size 0.8 mm, [0.4 – 2.7]), could be detected only due to their fluorescending properties (**Figure 9 c, d**) during fluorescence laparoscopy. The histological work-up of these specimens revealed alveolar RMS cells and tumor-free margins.
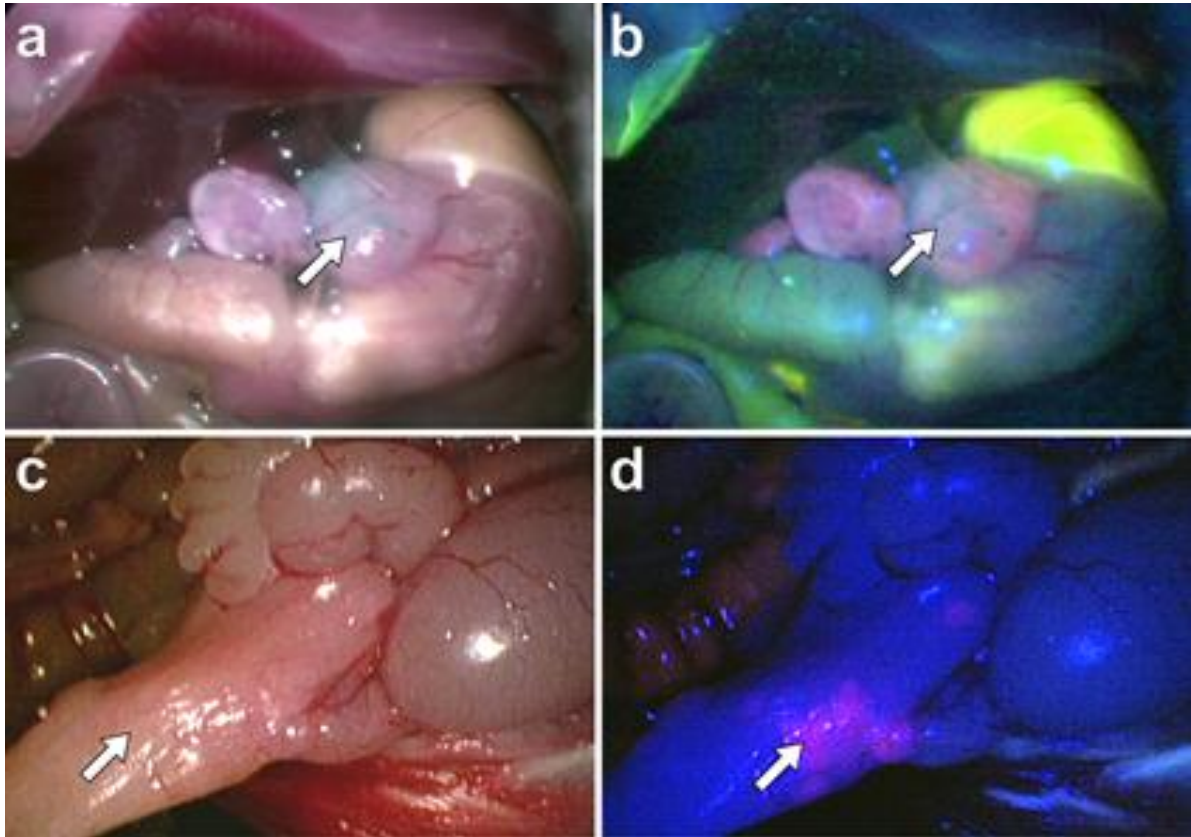
Figure 9. Appearance of the RMS tumors (arrow) located on the lesser curvature of the stomach as seen during conventional (**a**) and fluorescence laparoscopy (**b**). In the fat pad near the seminal vesicles, several tumors (arrow) with small dimensions and plane morphology (**c**) were missed by conventional laparoscopy but were detected under blue light based on their fluorescending behavior (**d**). Modified from (73)

Group II – Detection of RMS tumors based on their neovascularization using ICG-fluorescence laparoscopy (n=3)

In the second group, after xenotransplantation of non-transfected Rh30 cells, 20 tumors were detected in all mice (median 6 tumors [range 5-9] during conventional laparoscopy (WL mode) (**Figure 10 a)).** During examination with blue light (ICG mode) no fluorescence signals could be detected and the tumors appeared as dark spots (**Figure 10 b**). However, mesenteric blood vessels were clearly detected in the flooding phase of ICG. The fluorescence of ICG in the vessels persisted for approximately 10 minutes (**Figure 10 c**).
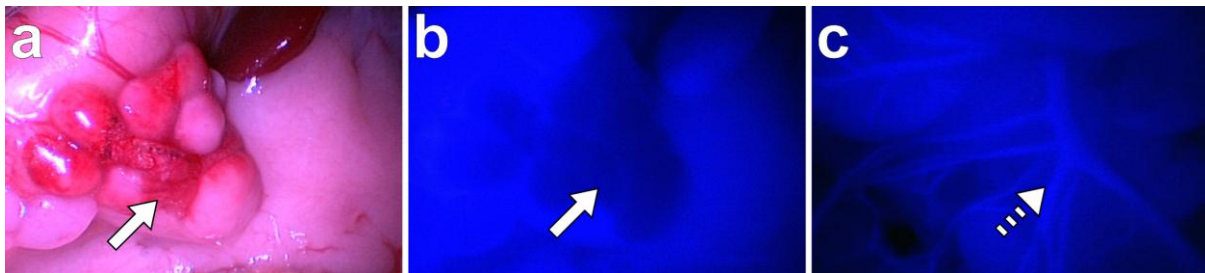

Figure 10. Tumors detected during the conventional laparoscopy (**a** – weighted arrow) did not accumulate ICG and appeared as dark areas during examination in ICG mode (**b** - weighted arrow). The mesenteric blood vessels (**c** – dotted arrow) were clearly seen during the flooding phase of ICG. Modified from (73)

Group III - Specific detection of RMS tumors based on their surface antigens using ICG-labeled cetuximab and fluorescence laparoscopy (n=4)

In this group, in order to increase the specificity of the method, ICG-Cetuximab was injected into the animals 24 hours prior to laparoscopy. No enhanced fluorescence could be detected in the tumors using the ICG mode (**Figure 11 b**). However, the *ex vivo* examination of the tumors using the Odissey system, revealed a successful binding of the ICG-labeled Cetuximab to the tumors cells as shown in **Figure 11 c**. In this group, a total number of twenty-four tumors in all

animals (median 6 tumors [2-10]) could be visualized during conventional laparoscopy (WL mode).
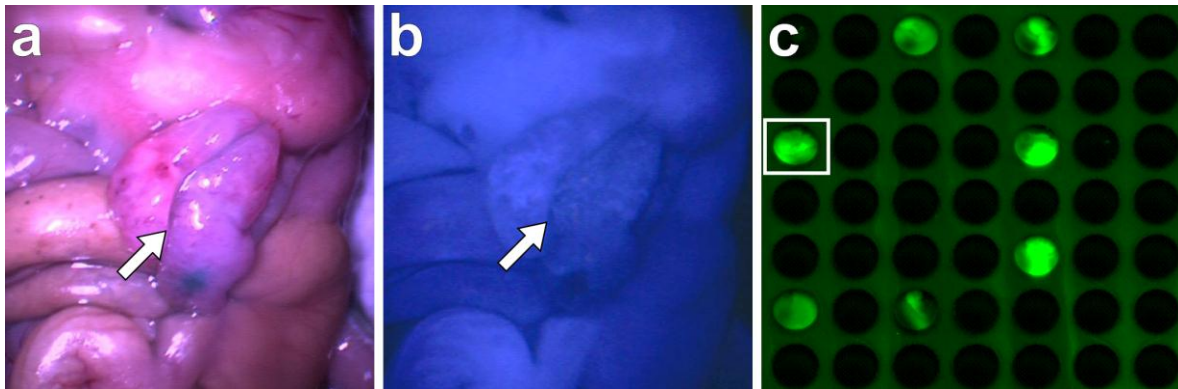

Figure 11. Accumulation of ICG-labeled cetuximab in the tumors (**a** - arrow) did not enhance the fluorescence of the tumor (**b** – arrow) during examination with blue light. The *ex vivo* examination using the Odissey system revealed a successful binding of the ICG-labeled cetuximab to RMS tumor cells (**c** – white box). Modified from (73)

Group IV – Detection of RMS tumors based on their hypericin uptake and using fluorescence laparoscopy (n=5)

In this group, during conventional laparoscopy (WL mode) 28 tumors (median 4 tumors/mouse [3-10]) were detected in all animals. Among these, 4 (median 1 tumor/mouse [0-2]) did not exhibit fluorescence during examination with blue light (AF mode) and were considered false positive. The histological examination of these structures revealed no RMS cells.

The remaining 24 tumors (median 3 tumors[2-10]) in all animals could be easily identified and differentiated from the healthy tissue due to a strong red fluorescence signal (**Figure 12 a, b**). These tumors had a median size of 4.4 mm [1.6 – 13.5] and a prominent appearance.

28 additional tumors in all 5 animals (median per animal: 10 tumors [7-18]) could be detected only during fluorescence laparoscopy based on their red fluorescence. They had a median size of 2.1 mm [0.5 – 11], and could not be distinguished from the surrounding tissue during conventional laparoscopy due to their plane morphology (**Figure 12 c, d**). The histological examination confirmed the presence of alveolar RMS cells in these tumors and also tumor free margins.
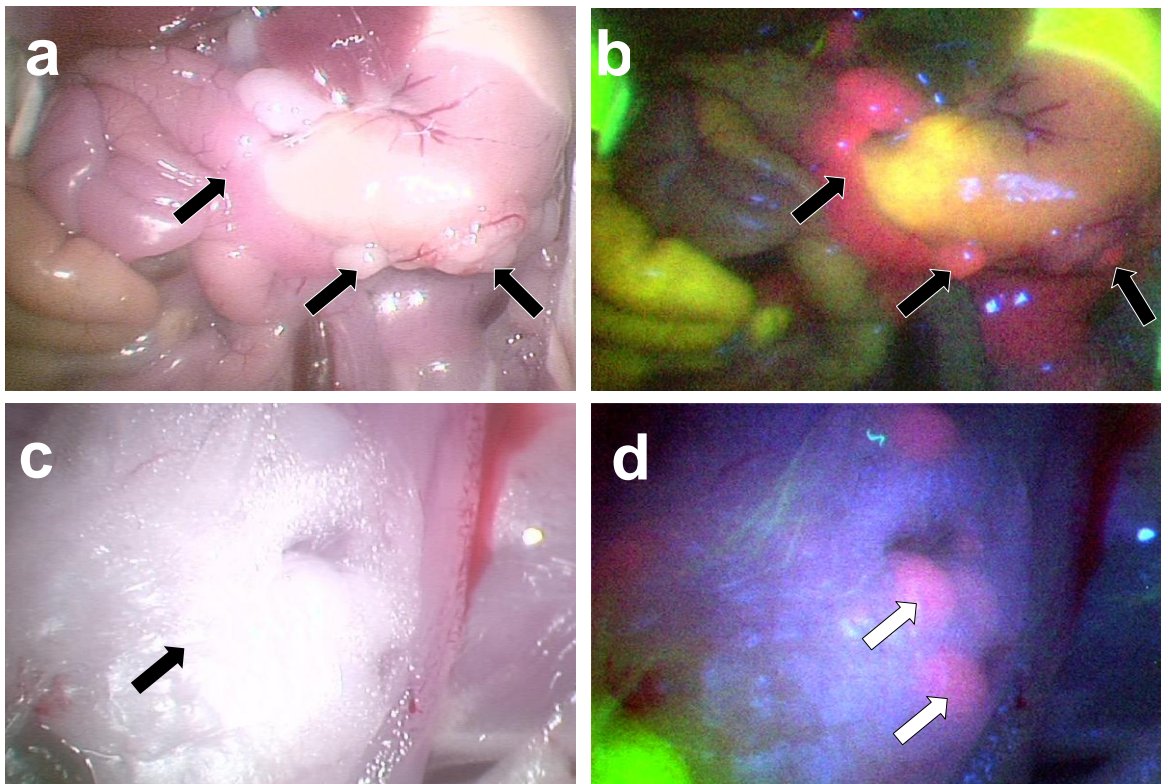
Figure 12. Aspect of RMS tumors (black arrows) located on the greater curvature of the stomach during conventional (**a**) and fluorescence laparoscopy (**b** - black arrows). The tumors with plane morphology and small dimensions localized in the lower abdomen (**c** - black arrow) which were missed by conventional laparoscopy (**c**), were clearly identified after administration of hypericin and examination in AF mode (**d** – white arrows). Modified from (73)

Effects of hypericin-induced photodynamic therapy

The TUNEL assay revealed the induction of apoptosis in almost all tumor cells (**Figure 13 a**). Additionally, apoptosis was also detected in the few healthy liver cells that were inadvertently exposed to blue light during laparoscopy (**Figure 13 b**) suggesting a possible damage of the liver exposed to blue light during the laparoscopic procedure.

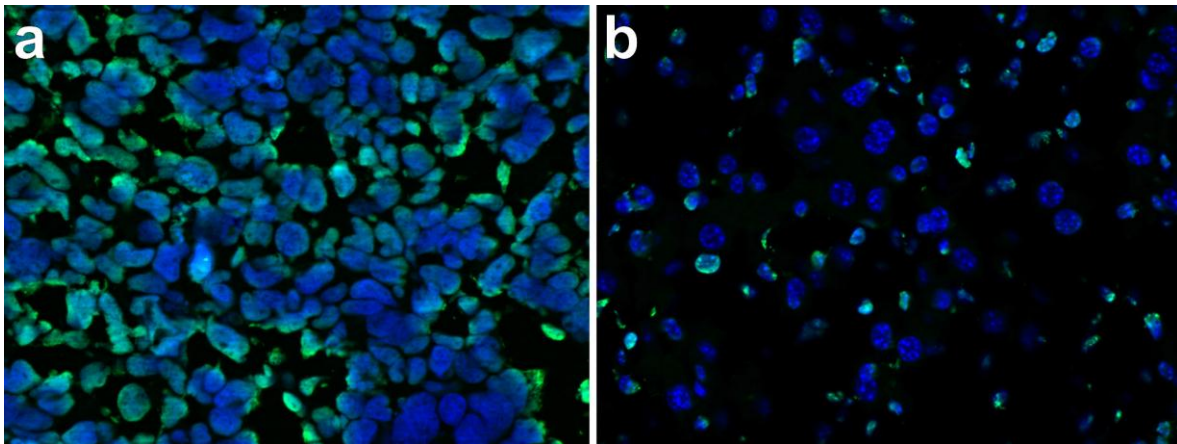**Figure 13.** TUNEL assay of the tumors **after PDT using hypericin.** The majority of the tumor cells were apoptotic(**a** - green). The counterstaining with DAPI revealed nuclei (**a** - blue) of all cells as marker of apoptosis. Apoptosis was also found in a lower degree in the areas of the liver which were inadvertently exposed to blue light during the procedure (**b** - green). Modified from (73).

DISCUSSION

Rhabdomyosarcoma is the most common soft tissue sarcoma and the third most common extracranial solid tumor of childhood, accounting for approximately 5% of all pediatric cancers (1, 4, 5).

The treatment of RMS is multimodal, including chemotherapy in conjunction with surgery, radiotherapy or a combination of both, in order to maximize local tumor control. The cooperative clinical groups from Europe (CWS Study Group, Italian Cooperative Group for pediatric STS, SIOP MMT Committee) and North America (STSC of the Children's Oncology Group) developed risk stratification systems to tailor treatment to need of patients.

It is due to the activity of these cooperative study trials that the survival of children suffering from RMS has improved dramatically over the last 30 years, from 25% in the early seventies to 70% nowadays. In the CWS experience, the low, standard and high risk group patients showed an EFS rate of 88%, 72% and 57%, and an OS rate of 97%, 95% and 67%, respectively (6). In the Italian Cooperative Group RMS-88 study, the overall 5-year EFS and OS were 65% and 74%, respectively (74), while in the MMT-89 study of the International Society of Pediatric Oncology the 5-year EFS and OS reached 57% and 71% (75). On the other side of the Atlantic, in the IRS Studies of the Children's Oncology Group the 5-year survival improved significantly from 55% on IRS-I and IRS-II studies to more than 70% on the IRS-III and IRS IV protocols (76).

However, the prognosis of the patients with high-risk disease remains poor with a 3-year event free survival (EFS) of less than 30% according to IRS studies (77). In the CWS-96 study, the survival of the patients with high-risk disease was better (5-year EFS 57% and OS 67%) but still remains poor (27).

Effective local control of the tumor is essential for the survival of patients with RMS. Thus, the main goal of the surgical treatment of RMS is the microscopically

complete tumor resection with avoidance of mutilating procedures. Due to a lack of clear delimitation between tumors and healthy tissue, especially in complex anatomical regions such as the pelvis, this objective is often difficult to accomplish. Thus, mutilating surgical procedures are sometimes required in order to achieve a complete tumor resection in order to prevent local recurrence.

Therefore, novel diagnostic and therapeutic modalities such as photodynamic diagnosis and therapy aiming to improve the intra-operative visualization of the tumors and their margins are required.

Based on the promising clinical results obtained in the field of urology in the detection of carcinoma in situ or small papillary tumors of the bladder (36), fluorescence diagnosis has also received significant interest in surgical oncology improving the early detection of breast, urogenital, pulmonary, and gastrointestinal tumors (33-37).

However, there are only few reports in the literature regarding fluorescence diagnosis for pediatric solid tumors. Successful tumor visualization using fluorescence laparoscopy with 5-ALA was reported in a rat model of xenotransplanted human hepatoblastoma (38). However, 5-ALA is known to rapidly bleach out and exposure to light is limited to short illumination periods. Additionally, the penetration into the tissue is low. Therefore, only superficial tumors can be detected. Moreover, it was not specified if complete tumor resection under fluorescence guidance was feasible in this model.

Our group has previously demonstrated that *in vivo* visualization of xenotransplanted pediatric RMS after transfection with red fluorescent protein (DsRed2) was effective (39). However, the potential clinical utility of fluorescending proteins in RMS is limited as they need to be bound to specific antibodies, which seems to be inapplicable in these tumors due to the absence of specific cell surface receptors. However, fluorescending agents represent an alternative for *in vivo* tumor visualization. In the present study, we used our mouse

model of disseminated pediatric RMS to evaluate the feasibility of fluorescence laparoscopy using different photosensitizers (mCherry, ICG and hypericin). This animal model resembles very well pediatric RMS in terms of organ invasion, intraperitoneal tumor spread, and difficulty to discriminate between tumor and surrounding tissue. The tumors exhibited strong fluorescence signals with an excellent contrast between the tumor margins and surrounding tissues using mCherry and hypericin. Therefore, both the identification of the tumors, based on their fluorescending behaviour, and their resection using fluorescence guidance could be carried out easily. In these groups, fluorescence laparoscopy resulted in a 1.6 fold increased tumor detection rate with a specificity of 100%. Comparable results were reported by other authors with Pp IX and 5-ALA fluorescence in a rat model of ovarian cancer (78) and disseminated colon carcinoma, respectively (79).

Indocyanine green (ICG) is a fluorescent agent currently used in cardiac, micro (circulatory) and liver function diagnosis (59). Together with methylene blue, they are the only near-infrared fluorophores that are registered with the Food and Drug Administration (FDA) and the European Medicines Agency (EMA) for clinical use. It has been shown that ICG passively accumulates in hepatocellular carcinoma and in non-cancerous hepatic parenchyma compressed by the colorectal liver metastases when intravenously administered between 1 and 14 days prior surgery (80). Thus, intraoperative fluorescence imaging techniques using ICG were developed and surgeons began to use them clinically to delineate cancers in the liver during open and laparoscopic hepatectomy (80-82). However, the major limitation of ICG fluorescence imaging is the inability to detect deeply located tumors. In the series of Kudo et al. none of the lesions located 8 mm or more from the liver capsule could be identified using ICG fluorescence (81).

In our model, using ICG, despite the good vascularisation of pediatric RMS, no fluorescence signals could be detected during ICG fluorescence laparoscopy. A possible reason might be the small dimensions of the tumors and their supplying blood vessels. During the histological examination of these tumors, we additionally

observed the presence of more vascular mimicry in contrast to "real" blood vessels. Vascular mimicry, also referred as vasculogenic mimicry, represents matrix-rich, non-endothelial-lined, vasculogenic-like channel networks responsible for the perfusion of certain types of tumors including alveolar RMS (83). Probably, the matrix-rich wall of these vascular-like channels might be responsible for the poor fluorescence signals obtained.

The chemical structure of ICG allows it to be conjugated with tumor specific antibodies (84). In order to improve the retention of ICG in RMS tumors, we labeled ICG to cetuximab, as our study group recently reported the successful binding of Cetuximab to RMS cells due to high expression of EGFR (40). We thought that targeting an antigen with higher density on the tumor cells may also enhance the fluorescence intensity leading to a better discrimination of the tumors. However, the results were not as expected. No enhancement of the ICG-fluorescence could be observed. Nevertheless, the *ex vivo* examination of the tumors using a laser-based system revealed a successful accumulation of the ICG-labeled cetuximab into the tumors. Similarly, Withrow and colleagues reported successful visualization of tumor cells, based on their binding to ICG labeled cetuximab and using a spectromicroscope in a mouse model of head and neck cancer (41). Therefore, the achieved density of fluorochrome-conjugated antibodies to tumor cells was not sufficient for the laparoscopic detection as the 3 mm laparoscope has been not currently optimized in NIR.

Using the Storz D-Light system (Karl Storz GmbH&Co., Tuttlingen, Germany), we could show that fluorescence laparoscopy is feasible and usable in our animal model. The laparoscopic procedure using the 3 mm laparoscope was well tolerated by the mice and no surgery-related death occurred. The fluorescence diagnosis was carried out without any difficulties as it could be easily switched between the different examination modes. However, the intensity of the fluorescence signal emitted by the tumors located between the intestinal loops or

between the stomach and the spleen was hampered to some extent probably due to autofluorescence of the nutrition or absorption of the excitation light by these structures. Therefore, for an adequate exposure of the fluorescending tumors, the mobilization of these organs was necessary. A laser light source, resulting in a decreased excitation light leakage and higher signal-to-noise-ratio or an optical instrument having a better resolution may improve the detection of these tumors.

We find that this system has two major advantages. First of all this system can be also adapted for conventional open surgical approaches. Due to the small dimensions of the mice, the resection of the tumors was carried out by a laparotomy using fluorescence guidance. A clear identification of the tumor margins based on the red fluorescence of the tumors was possible in this setting and the complete resection of the tumors (macroscopically and microscopically) was carried out without any difficulties. However, in humans, the operative field is larger compared to the mouse. Therefore, the amount of light delivered by the small light source of the endoscope may be insufficient for appropriate excitation and consequently the fluorescence signal may be weak. However, this impairment may be overcome by using an exoscopic video camera (VITOM®, Karl Storz GmbH&Co., Tuttlingen, Germany) which provides an external view of the operative field with a two fold magnification. VITOM® is a specially designed scope that is attached to a high definition digital camera and displayed on a HD video monitor. It is used in neurosurgery as an alternative to the operating microscope (85).

The second major advantage of the system is that fluorescence laparoscopy can be combined with PDT at the same time for the local therapy of remnant microscopic tumors.

Photodynamic therapy involves the systemic or topical administration of a photosensitizer resulting in a selective accumulation in the cancer cells. Excitation

with light of the appropriate wave length results in generation of a highly reactive oxygen species leading to tumor cell apoptosis. There are many reports demonstrating the effectiveness of this method as a novel treatment option for various malignancies (47, 48, 50, 70, 86). The main photosensitizers used are 5-ALA and hypericin.

Hypericin is a hydroxylated phenantroperylenequinone derivate, isolated from plants of St. John's Wort (*Hypericum perforatum*) (54). It has primarly been used for the treatment of depressive disorders (45, 64). Hypericin has been described for *in vivo* visualization of bladder cancer (62) and has been studied as a photodynamic agent in different tumor entities (63, 64, 66, 68). Some of these studies revealed also impressive anti-angiogenic effects (66, 68). Interestingly, some authors reported anti-metastatic and anti-angiogenic effects of hypericin even in the dark (87, 88). Ritz demonstrated even that hypericin has a higher phototoxicity and fluorescence compared with 5 ALA, for photodynamic inactivation of medulloblastoma cells (51). Thus, hypericin seems to be a better photodynamic agent compared with 5-ALA.

There is a lack of reports in the literature about PDT in RMS. In our previous investigations we demonstrated that *in vitro* photoactivation of hypericin led to apoptosis of rhabdomyosarcoma and epithelial liver tumor cells (47, 55). Our present results demonstrate that hypericin-induced photodynamic therapy on childhood rhabdomyosarcoma is also possible *in vivo* as PDT with hypericin resulted in induction of apoptosis in the tumor samples. The TUNEL test was positive in almost all tumor cells 4 hours after induction of PDT. These findings show that hypericin specifically accumulates in RMS cells *in vivo*. To our knowledge, this is the first report in the literature, which demonstrates that PDT with hypericin is also possible *in vivo* in pediatric RMS (73).

Although hypericin uptake is thought to be tumor specific (47), few apoptotic bodies were observed also in the hepatic tissue inadvertently exposed to blue light

during laparoscopy. Therefore, the protection of the tissue with high proliferative activity (e.g. liver in children) during the procedure with an opaque sheet seems to be necessary.

Complications after photodynamic therapy were reported by other authors. De Laney et al. encountered three small bowel perforations after PDT with 2.5 mg/kg dihematoporphirin ethers (DHE) and light dose of $3J/cm^2$ in a phase I study of debulking surgery for disseminated intraperitoneal tumors. In one patient, further increase of the light dose used for PDT determined a gastric perforation and pleural effusion requiring thoracocentesis (89). Regarding hypericin, animal studies in mice showed no severe side effects of the drug if the animals were kept in the dark (54, 90). Moreover, hypericin is already clinically used in different tumor entities such as bladder carcinoma and glioblastoma without severe side effects (62, 91).

One of the most important side effects of hypericin PDT is hypericism, which is a severe photodermatitis observed in grazing animals and cause by the UV light exposure after ingestion of St John's Wort (92). Animal hypericism ranges from erythema of the skin exposed to UV light to extensive rashes with vesiculation, edema and fever to behavioral changes, seizures and death. In humans, recent pharmacokinetic studies suggest that the phototoxic threshold level of hypericin is not reached with dosages used for the oral treatment of depression (900 - 3600 mg of hypericin extract, equivalent of 2.8 mg - 11.25 mg hypericin plus pseudohypericin) (93). However, preparations containing hypericin which are used as an antidepressant are largerly unregulated and contain varying amounts of the drug (94). While studying the antiretroviral effects of hypericin on HIV infected patients, Gulik et al reported that all patients treated with hypericin experienced phototoxicity if the dosage was higher than 0.25 mg/kg twice weekly, administered intravenously. The toxic reaction was an erythematous rash associated with painful dysesthesias that involved areas exposed to light (94). The reaction resolved after discontinuation of the therapy. However, the doses used for

intraoperative visualization and PDT are considerably lower (0.1 mg/kg) (91, 95), therefore major side effects of hypericin should not be expected. Ritz et al. studying the intraoperative visualization of malignant glioma after injection of hypericin reported no side effects or phototoxic reactions after intravenous administration of 0.1mg/kg hypericin (91). St John's Wort preparations may cause drug interactions through the induction of the cytochrome P450 enzymes resulting in the increased metabolism of the drugs such as digoxin (96), theophylline or cyclosporine (97). This leads to decreased plasma concentration and clinical effects of these drugs (92).

The indirect effects of hypericin-induced photodynamic therapy have also been shown to contribute to tumor destruction. Necrosis of the tumor due to vascular compromise when high intravascular concentrations of hypericin were present at the time of photoactivation was demonstrated by Chen et al in a tumor model of radiation-induced fibrosarcoma (RIF-1). The immune system also seems to play a role in tumor destruction by activation of inflammatory cells following PDT (98), since less tumor damage occurred in mice treated with cyclosporin A prior to PDT as described by Eastin et al (99). In our model, due to low vascularisation of the tumors and highly immunosuppressed mice, these aspects of PDT could not be assessed.

As a possible translational approach, integration of hypericin in RMS surgery can be achieved without major changes. Injection of hypericin prior to surgery may allow a better detection of the tumor margins to facilitate microscopically complete tumor resections. Ritz et al recently reported the successful fluorescence-guided resection of recurrent malignant gliomas using an injectable solution of hypericin (91). PDT of incomplete resection margins may also improve the outcome of the patients due to the destruction of microscopical residuals. Intraoperative PDT could either be carried out during laparoscopy or during open tumor resections with specific filters in the OR lighting system.

While studying the differences in metabolic pathways in rhabdomyosarcoma Rh 30 cells and human primary myocites *in vitro* using stable isotope tracing methods, Fan et al observed that in Rh 30 cells, glycolysis, Kreb's cycle pentose phosphate pathway as well as nucleotide biosynthesis were enhanced compared with normal myocites, in order to meet the demand for accelerated growth. They also showed that the mitochondria of Rh 30 cells are active both in Kreb's cycle and respiratory electron transport and postulated that these processes may be responsible for the transformation of primary myocites into malignant cells (100). Electrochemical studies demonstrated that hypericin is capable of either accepting or donating electrons, thus functioning as both oxidizing and reducing agent, which may facilitate activities in the dark as well. Several studies revealed the anti-metastatic and anti-angiogenic effects of hypericin in the dark (87, 88).

Finally, we conclude that fluorescence laparoscopy is a promising novel tool for *in vivo* diagnosis and photodynamic therapy of childhood rhabdomyosarcoma. The first steps for a translation into the clinic were taken by developing and using injectable hypericin (91, 101). Therefore, a clinical trial will now be initiated in children suffering from advanced-stage RMS.

SUMMARY

Rhabdomyosarcoma is the most common soft tissue sarcoma in children. The multimodal treatment resulted in an increased survival rate of patients with localized disease. However, the prognosis of children in advanced stages of the disease remains poor. Local control of the tumor is essential for the survival of these patients. Surgery plays a key role in the local treatment of RMS. The main problem remains the lack of clear identification of tumor margins, especially in complex anatomical regions. This sometimes leads to mutilating surgical procedures to acquire a R0 resection in order to prevent local tumor recurrence. To overcome this major problem, novel diagnostic and therapeutic approaches aiming to improve the intraoperative tumor visualization are necessary.

Photodynamic diagnosis represents a novel technique aiming to improve the intraoperative tumor detection. The principle of PDD is based on the accumulation of a photosensitizer in the tumor cells. The interaction of light of specific wavelength with the tumor causes the fluorescence of the photosensitizer, thus resulting in easy identification of the tumor. Using this technique, promising results were obtained in surgical oncology regarding early detection of various malignancies. The most commonly used substances to this purpose are 5-ALA (with its derivatives) and hypericin. There are many reports which demonstrate the superiority of hypericin to ALA regarding photostability.

In the present study, fluorescence laparoscopy using hypericin resulted in a 1.6 increased tumor detection rate with a specificity of 100%. The tumors exhibited strong fluorescence signals and an excellent contrast between tumor margins and healthy tissue. Thus, the identification and resection of the tumors under fluorescence guidance could be carried out easily. This is the first report in the literature on *in vivo* PDD in pediatric RMS.

Besides its fluorescending properties, hypericin is also known as a very potent photodynamic agent. After activation with light of appropriate wavelength it

produces singlet oxygen efficiently, resulting in apoptosis of the tumor cells. Successful *in vitro* hypericin-induced PDT of RMS cells was previously reported by our study group. In the present study we demonstrated that hypericin-induced PDT is also possible *in vivo*. Photodynamic therapy after photosensitization with hypericin resulted in the induction of apoptosis in almost all tumor cells. This suggests that hypericin specifically accumulates in RMS cells *in vivo*. This is the first report on *in vivo* hypericin-induced PDT in pediatric RMS.

The integration of hypericin in RMS surgery can be achieved without major difficulties. The first step for translation into the clinic was done by developing injectable hypericin. Moreover, hypericin is already clinically used in different tumor entities without major side effects. The injection of hypericin prior to surgery may allow a better detection of tumor margins, possibly resulting in R0 tumor resections. Furthermore, fluorescence laparoscopy can be combined with PDT at the same time for the local therapy of incomplete resection margins. This may improve the outcome of the patients due to destruction of microscopic residuals. Intraoperative PDD and PDT are possible either during laparoscopy or in the setting of open surgery using specific filters in the OR lighting system.

In conclusion, fluorescence laparoscopy is a promising novel tool for *in vivo* PDD and PDT of pediatric RMS. Therefore, a clinical trial will now be initiated in children suffering from advanced-stage RMS.

ZUSAMMENFASSUNG

Das Rhabdomyosarkom ist das häufigste Weichteilsarkom im Kindesalter. Die multimodale Therapie führte zu einer erhöhten Überlebensrate des Patienten mit lokalisierter Erkrankung. Die Prognose im fortgeschrittenen Tumorstadium ist jedoch bis heute sehr schlecht. Die Detektion und die vollständige Entfernung der Tumoren sind für eine erfolgreiche Therapie essentiell. Deshalb spielt die Chirurgie in der lokalen Behandlung dieser Tumoren eine wichtige Rolle. Das Hauptproblem in der Chirurgie des Rhabdomyosarkoms ist, dass die Resektionsgrenzen nicht eindeutig identifiziert werden können. Daraus resultiert, dass in manchen Fällen die Tumoren nur durch eine mutilierende Operation reseziert werden können. Dennoch verbleibt ein Restrisiko mikroskopische Tumorreste zu belassen. Die genaue intraoperative Detektion von Tumoren und vor allem ihrer Grenzen in anatomisch komplexen Regionen durch optische Hilfsmittel wäre ein wichtiger Schritt in der Tumorchirurgie.

Die photodynamische Diagnostik (PDD) oder Fluoreszenzdiagnostik ist ein relativ neues Verfahren für Verbesserung der intraoperativen Tumordetektion. Diese Methode basiert auf die Akkumulation von photodynamisch aktiven Substanzen (Photosensibilisatoren) in den Tumorzellen. Daraus resultiert eine Verbesserung des optischen Kontrastes zwischen Tumor und den umgebenden Gewebe. Hypericin ist eine hierfür am häufigsten verwendeten Substanzen. Bisher existieren keine wissenschaftliche Untersuchungen zur *in vivo* Fluoreszenzdiagnostik mit Hypericin bei kindlichen RMS. In der vorliegenden Studie konnte beobachtet werden, dass die Fluoreszenzlaparoskopie mit Hypericin zu einer 1.6 erhöhten Tumoridentifikationsrate bei einer Spezifizität von 100% geführt hat. Die Identifizierung und die Resektion der Tumoren konnte problemlos aufgrund deren Fluoreszenzenz durchgeführt werden. Dies ist der erste Bericht in der Literatur über die *in vivo* Fluoreszenzlaparoskopie bei kindlichen RMS.

Neben der positiven Eigenschaften von Hypericin in der photodynamischen Diagnostik, kann es auch für die photodynamische Therapie eingesetzt werden. Hierbei kommt es durch die Anregung mit Licht einer bestimmten Wellenlänge zur Bildung von Sauerstoffradikalen. In dieser Studie haben wir beobachtet, dass die intraoperative PDT mit Hypericin zur Induktion der Apoptose in fast alle Tumorzellen geführt hat. Unsere Beobachtung legen daher nahe, dass die Hypericin sich spezifisch in RMS Zellen in vivo akkumuliert.

Der Einsatz von Hypericin in der Klinik kann ohne große Veränderungen erreicht werden. Der erste Schritt für den Einsatz in der Klinik wurde durch die Entwicklung einer Hypericin-Injektionslösung realisiert. Darüber hinaus wird Hypericin bereits klinisch bei verschiedenen Tumorentitäten verwendet. Die Fluoreszenzlaparoskopie kann zusammen mit der PDT kombiniert werden. Nach der Aufnahme von Hypericin in den RMS Zellen könnte das OP-Licht zur Visualisierung der Tumorgrenzen und zur Induktion der PDT verwendet werden. Intraoperative PDD und PDT sind entweder während der Laparoskopie oder in Rahmen eines offen chirurgischen Eingriffs möglich.

Zusammenfassend ist die Floreszenzlaparoskopie eine sehr versprechende Methode für die intraoperative Tumordetektion. Die PDT mit Hypericin stellt eine potentielle neue Therapieoption zur Behandlung des kindlichen RMS dar, welche sowohl eine bessere intraoperative Tumoridentifizierung als auch eine intraoperative Therapieoption darstellen könnte. Deshalb wird nun eine klinische Studie bei kindlichen mit fortgeschrittenem Tumorsstadium initiiert werden.

REFERENCES

1. Andrassy R. Soft tissue sarcoma. In: Carachi R, Grosfeld, J., Azmy, A. The surgery of childhood tumors. Berlin: Springer-Verlag; 2008. p 273-297.

2. Rodeberg DPaidas C. Childhood rhabdomyosarcoma. Seminars in pediatric surgery 2006:15:57-62.

3. Weihkopf T, Blettner M, Dantonello T, et al. Incidence and time trends of soft tissue sarcomas in german children 1985-2004 - a report from the population-based german childhood cancer registry. European journal of cancer (Oxford, England : 1990) 2008:44:432-440.

4. Dasgupta RRodeberg DA. Update on rhabdomyosarcoma. Seminars in pediatric surgery 2012:21:68-78.

5. Huh WWSkapek SX. Childhood rhabdomyosarcoma: New insight on biology and treatment. Current oncology reports 2010:12:402-410.

6. Koscielniak E, Kliengebiel, T. Cws guidance for risk adapted treatment of soft tissue sarcoma and soft tissue tumors in children, adolescents and young adults. Stuttgart, Germany: Cooperative Weichteilsarkom Studiengruppe (CWS) of the Gesellschaft für Pädiatrische Onkologie und Hämatologie (GPOH); 2014. p.

7. Cocker HA, Pinkerton CRKelland LR. Characterization and modulation of drug resistance of human paediatric rhabdomyosarcoma cell lines. British journal of cancer 2000:83:338-345.

8. Enzinger FM, Weiss, S.W. Soft tissue tumors. In: Enzinger FM, Weiss, S.W. Soft tissue tumors. St. Louis, USA: CV Mosby Co; 1995. p

9. Koscielniak EF, J. Weichteiltumoren - rhabdomyosarkomen. In: Fuchs J. Solide tumoren im kindesalter. Stuttgart, Germany: Schattauer GmbH; 2012. p 201-232.

10. Barr FG. Molecular genetics and pathogenesis of rhabdomyosarcoma. Journal of pediatric hematology/oncology 1997:19:483-491.

11. Kelly KM, Womer RB, Sorensen PH, et al. Common and variant gene fusions predict distinct clinical phenotypes in rhabdomyosarcoma. Journal of clinical oncology : official journal of the American Society of Clinical Oncology 1997:15:1831-1836.

12. Cao L, Yu Y, Bilke S, et al. Genome-wide identification of pax3-fkhr binding sites in rhabdomyosarcoma reveals candidate target genes important for development and cancer. Cancer research 2010:70:6497-6508.

13. Davicioni E, Anderson MJ, Finckenstein FG, et al. Molecular classification of rhabdomyosarcoma--genotypic and phenotypic determinants of diagnosis: A report from the children's oncology group. The American journal of pathology 2009:174:550-564.

14. Rudzinski ER, Teot LA, Anderson JR, et al. Dense pattern of embryonal rhabdomyosarcoma, a lesion easily confused with alveolar rhabdomyosarcoma: A report from the soft tissue sarcoma committee of the children's oncology group. American journal of clinical pathology 2013:140:82-90.

15. Barr FG, Qualman SJ, Macris MH, et al. Genetic heterogeneity in the alveolar rhabdomyosarcoma subset without typical gene fusions. Cancer research 2002:62:4704-4710.

16. Xia SJ, Pressey JGBarr FG. Molecular pathogenesis of rhabdomyosarcoma. Cancer biology & therapy 2002:1:97-104.

17. Williamson D, Missiaglia E, de Reynies A, et al. Fusion gene-negative alveolar rhabdomyosarcoma is clinically and molecularly indistinguishable from embryonal rhabdomyosarcoma. Journal of clinical oncology : official journal of the American Society of Clinical Oncology 2010:28:2151-2158.

18. Wachtel M, Dettling M, Koscielniak E, et al. Gene expression signatures identify rhabdomyosarcoma subtypes and detect a novel t(2;2)(q35;p23) translocation fusing pax3 to ncoa1. Cancer research 2004:64:5539-5545.

19. Missiaglia E, Williamson D, Chisholm J, et al. Pax3/foxo1 fusion gene status is the key prognostic molecular marker in rhabdomyosarcoma and significantly improves current risk stratification. Journal of clinical oncology : official journal of the American Society of Clinical Oncology 2012:30:1670-1677.

20. Wexler LHLadanyi M. Diagnosing alveolar rhabdomyosarcoma: Morphology must be coupled with fusion confirmation. Journal of clinical oncology : official journal of the American Society of Clinical Oncology 2010:28:2126-2128.

21. Anderson JR, Barr FG, Hawkins DS, et al. Fusion-negative alveolar rhabdomyosarcoma: Modification of risk stratification is premature. Journal of clinical oncology : official journal of the American Society of Clinical Oncology 2010:28:e587-588; author reply e589-590.

22. De Giovanni C, Landuzzi L, Nicoletti G, et al. Molecular and cellular biology of rhabdomyosarcoma. Future oncology (London, England) 2009:5:1449-1475.

23. Modritz D, Ladenstein R, Potschger U, et al. Treatment for soft tissue sarcoma in childhood and adolescence. Austrian results within the cws 96 study. Wiener klinische Wochenschrift 2005:117:196-209.

24. Dantonello TM, Int-Veen C, Winkler P, et al. Initial patient characteristics can predict pattern and risk of relapse in localized rhabdomyosarcoma. Journal of clinical oncology : official journal of the American Society of Clinical Oncology 2008:26:406-413.

25. Wolden SL, Anderson JR, Crist WM, et al. Indications for radiotherapy and chemotherapy after complete resection in rhabdomyosarcoma: A report from the intergroup rhabdomyosarcoma studies i to iii. Journal of clinical oncology : official journal of the American Society of Clinical Oncology 1999:17:3468-3475.

26. Schuck A, Mattke AC, Schmidt B, et al. Group ii rhabdomyosarcoma and rhabdomyosarcomalike tumors: Is radiotherapy necessary? Journal of clinical oncology : official journal of the American Society of Clinical Oncology 2004:22:143-149.

27. (GPOH) GfPOuH. Cooperative weichteilsarkom studie cws-2002 p. Stuttgart: 2003. p.

28. Koscielniak E, Harms D, Henze G, et al. Results of treatment for soft tissue sarcoma in childhood and adolescence: A final report of the german cooperative soft tissue sarcoma study cws-86. Journal of clinical oncology : official journal of the American Society of Clinical Oncology 1999:17:3706-3719.

29. Seitz G, Dantonello TM, Int-Veen C, et al. Treatment efficiency, outcome and surgical treatment problems in patients suffering from localized embryonal bladder/prostate rhabdomyosarcoma: A report from the cooperative soft tissue sarcoma trial cws-96. Pediatric blood & cancer 2011:56:718-724.

30. Klingebiel T, Pertl U, Hess CF, et al. Treatment of children with relapsed soft tissue sarcoma: Report of the german cess/cws rez 91 trial. Medical and pediatric oncology 1998:30:269-275.

31. Arndt C, Rodeberg D, Breitfeld PP, et al. Does bladder preservation (as a surgical principle) lead to retaining bladder function in bladder/prostate rhabdomyosarcoma? Results from intergroup rhabdomyosarcoma study iv. The Journal of urology 2004:171:2396-2403.

32. Jichlinski PLeisinger HJ. Fluorescence cystoscopy in the management of bladder cancer: A help for the urologist! Urologia internationalis 2005:74:97-101.

33. Chan JK, Monk BJ, Cuccia D, et al. Laparoscopic photodynamic diagnosis of ovarian cancer using 5-aminolevulinic acid in a rat model. Gynecologic oncology 2002:87:64-70.

34. Orth K, Russ D, Steiner R, et al. Fluorescence detection of small gastrointestinal tumours: Principles, technique, first clinical experience. Langenbeck's archives of surgery / Deutsche Gesellschaft fur Chirurgie 2000:385:488-494.

35. Ladner DP, Steiner RA, Allemann J, et al. Photodynamic diagnosis of breast tumours after oral application of aminolevulinic acid. British journal of cancer 2001:84:33-37.

36. Kriegmair M, Baumgartner R, Knuchel R, et al. Detection of early bladder cancer by 5-aminolevulinic acid induced porphyrin fluorescence. The Journal of urology 1996:155:105-109; discussion 109-110.

37. Leunig A, Rick K, Stepp H, et al. Fluorescence imaging and spectroscopy of 5-aminolevulinic acid induced protoporphyrin ix for the detection of neoplastic lesions in the oral cavity. American journal of surgery 1996:172:674-677.

38. Till H, Bergmann F, Metzger R, et al. Videoscopic fluorescence diagnosis of peritoneal and thoracic metastases from human hepatoblastoma in nude rats. Surgical endoscopy 2005:19:1483-1486.

39. Seitz G, Warmann SW, Fuchs J, et al. Visualization of xenotransplanted human rhabdomyosarcoma after transfection with red fluorescent protein. Journal of pediatric surgery 2006:41:1369-1376.

40. Herrmann D, Seitz G, Warmann SW, et al. Cetuximab promotes immunotoxicity against rhabdomyosarcoma in vitro. Journal of immunotherapy (Hagerstown, Md : 1997) 2010:33:279-286.

41. Withrow KP, Gleysteen JP, Safavy A, et al. Assessment of indocyanine green-labeled cetuximab to detect xenografted head and neck cancer cell lines. Otolaryngology--head and neck surgery : official journal of American Academy of Otolaryngology-Head and Neck Surgery 2007:137:729-734.

42. Hornung R, Major AL, McHale M, et al. In vivo detection of metastatic ovarian cancer by means of 5-aminolevulinic acid-induced fluorescence in a rat model. The Journal of the American Association of Gynecologic Laparoscopists 1998:5:141-148.

43. Stummer W, Pichlmeier U, Meinel T, et al. Fluorescence-guided surgery with 5-aminolevulinic acid for resection of malignant glioma: A randomised controlled multicentre phase iii trial. The lancet oncology 2006:7:392-401.

44. Stummer W, Beck T, Beyer W, et al. Long-sustaining response in a patient with non-resectable, distant recurrence of glioblastoma multiforme treated by interstitial photodynamic therapy using 5-ala: Case report. Journal of neuro-oncology 2008:87:103-109.

45. Wada A, Sakaeda T, Takara K, et al. Effects of st john's wort and hypericin on cytotoxicity of anticancer drugs. Drug metabolism and pharmacokinetics 2002:17:467-474.

46. D'Hallewin MA, De Witte PA, Waelkens E, et al. Fluorescence detection of flat bladder carcinoma in situ after intravesical instillation of hypericin. The Journal of urology 2000:164:349-351.

47. Seitz G, Warmann SW, Armeanu S, et al. In vitro photodynamic therapy of childhood rhabdomyosarcoma. International journal of oncology 2007:30:615-620.

48. Hendrickx N, Volanti C, Moens U, et al. Up-regulation of cyclooxygenase-2 and apoptosis resistance by p38 mapk in hypericin-mediated photodynamic therapy of human cancer cells. The Journal of biological chemistry 2003:278:52231-52239.

49. Ritz R, Muller M, Weller M, et al. Hypericin: A promising fluorescence marker for differentiating between glioblastoma and neurons in vitro. International journal of oncology 2005:27:1543-1549.

50. Du HY, Bay BHOlivo M. Biodistribution and photodynamic therapy with hypericin in a human npc murine tumor model. International journal of oncology 2003:22:1019-1024.

51. Ritz R, Scheidle C, Noell S, et al. In vitro comparison of hypericin and 5-aminolevulinic acid-derived protoporphyrin ix for photodynamic inactivation of medulloblastoma cells. PloS one 2012:7:e51974.

52. Chen B, Xu Y, Roskams T, et al. Efficacy of antitumoral photodynamic therapy with hypericin: Relationship between biodistribution and photodynamic effects in the rif-1 mouse tumor model. International journal of cancer Journal international du cancer 2001:93:275-282.

53. H R. Formation d'oxygène singulet 1 delta g photosensibilisée par l'hypericine; étude cinétique en milieu micellaire non ionique. J Chem Phys Chim Biol 1988:971-976.

54. Kamuhabwa A, Agostinis P, Ahmed B, et al. Hypericin as a potential phototherapeutic agent in superficial transitional cell carcinoma of the bladder. Photochemical & photobiological sciences : Official journal of the European Photochemistry Association and the European Society for Photobiology 2004:3:772-780.

55. Seitz G, Krause R, Fuchs J, et al. In vitro photodynamic therapy in pediatric epithelial liver tumors promoted by hypericin. Oncology reports 2008:20:1277-1282.

56. Hermann D. Immuntherapeutische ansätze beim rhabdomyosarkom: Therapeutische antikörper und phagozytose. thesis. Mathematisch-Naturwissenschaftlichen Fakultät Eberhard Karl Universität Tübingen 2011. 151 p.

57. Shaner NC, Campbell RE, Steinbach PA, et al. Improved monomeric red, orange and yellow fluorescent proteins derived from discosoma sp. Red fluorescent protein. Nature biotechnology 2004:22:1567-1572.

58. Shaner NC, Steinbach PATsien RY. A guide to choosing fluorescent proteins. Nature methods 2005:2:905-909.

59. Betz CS, Zhorzel S, Schachenmayr H, et al. Endoscopic measurements of free-flap perfusion in the head and neck region using red-excited indocyanine green: Preliminary results. Journal of plastic, reconstructive & aesthetic surgery : JPRAS 2009:62:1602-1608.

60. Litvack ZN, Zada GLaws ER, Jr. Indocyanine green fluorescence endoscopy for visual differentiation of pituitary tumor from surrounding structures. Journal of neurosurgery 2012:116:935-941.

61. Yamamoto M, Kazumasa, O., Takayuki, S. . Intraoperative indocyanine green imaging technique in cardiovascular surgery. In: Aronov WS. Artery bypass. InTech; 2013. p

62. D'Hallewin MA, Kamuhabwa AR, Roskams T, et al. Hypericin-based fluorescence diagnosis of bladder carcinoma. BJU international 2002:89:760-763.

63. Kamuhabwa AA, Di Mavungu JD, Baert L, et al. Determination of hypericin in human plasma by high-performance liquid chromatography after intravesical administration in patients with transitional cell carcinoma of the bladder. European journal of pharmaceutics and biopharmaceutics : official journal of Arbeitsgemeinschaft fur Pharmazeutische Verfahrenstechnik eV 2005:59:469-474.

64. Tian R, Koyabu N, Morimoto S, et al. Functional induction and de-induction of p-glycoprotein by st. John's wort and its ingredients in a human colon adenocarcinoma cell line. Drug metabolism and disposition: the biological fate of chemicals 2005:33:547-554.

65. VanderWerf QM, Saxton RE, Chang A, et al. Hypericin: A new laser phototargeting agent for human cancer cells. The Laryngoscope 1996:106:479-483.

66. Sarissky M, Lavicka J, Kocanova S, et al. Diazepam enhances hypericin-induced photocytotoxicity and apoptosis in human glioblastoma cells. Neoplasma 2005:52:352-359.

67. Chen B, Roskams Tde Witte PA. Antivascular tumor eradication by hypericin-mediated photodynamic therapy. Photochemistry and photobiology 2002:76:509-513.

68. Yee KK, Soo KCOlivo M. Anti-angiogenic effects of hypericin-photodynamic therapy in combination with celebrex in the treatment of human nasopharyngeal carcinoma. International journal of molecular medicine 2005:16:993-1002.

69. Alander JT, Kaartinen I, Laakso A, et al. A review of indocyanine green fluorescent imaging in surgery. International journal of biomedical imaging 2012:2012:940585.

70. Head CS, Luu Q, Sercarz J, et al. Photodynamic therapy and tumor imaging of hypericin-treated squamous cell carcinoma. World journal of surgical oncology 2006:4:87.

71. Shultz LD, Lyons BL, Burzenski LM, et al. Human lymphoid and myeloid cell development in nod/ltsz-scid il2r gamma null mice engrafted with mobilized human hemopoietic stem cells. Journal of immunology (Baltimore, Md : 1950) 2005:174:6477-6489.

72. Ganti R, Skapek SX, Zhang J, et al. Expression and genomic status of egfr and erbb-2 in alveolar and embryonal rhabdomyosarcoma. Modern pathology : an official journal of the United States and Canadian Academy of Pathology, Inc 2006:19:1213-1220.

73. Urla C. A-ES, Fuchs J., Seitz G. Successful in vivo tumor visualization using fluorescence laparoscopy in a mouse model of disseminated alveolar rhabdomyosarcoma. Surgical endoscopy 2014:in print:

74. Carli M, Bisogno GCecchetto G. Childhood rhabdomyosarcoma: Results of the italian cooperative study rms88. Medical and pediatric oncology 1998:31:262.

75. Stevens MC, Rey A, Bouvet N, et al. Treatment of nonmetastatic rhabdomyosarcoma in childhood and adolescence: Third study of the international society of paediatric oncology--siop malignant mesenchymal tumor 89. Journal of clinical oncology : official journal of the American Society of Clinical Oncology 2005:23:2618-2628.

76. Pappo AS, Shapiro DN, Crist WM, et al. Biology and therapy of pediatric rhabdomyosarcoma. Journal of clinical oncology : official journal of the American Society of Clinical Oncology 1995:13:2123-2139.

77. Hayes-Jordan AAndrassy R. Rhabdomyosarcoma in children. Current opinion in pediatrics 2009:21:373-378.

78. Ludicke F, Gabrecht T, Lange N, et al. Photodynamic diagnosis of ovarian cancer using hexaminolaevulinate: A preclinical study. British journal of cancer 2003:88:1780-1784.

79. Gahlen J, Stern J, Laubach HH, et al. Improving diagnostic staging laparoscopy using intraperitoneal lavage of delta-aminolevulinic acid (ala) for laparoscopic fluorescence diagnosis. Surgery 1999:126:469-473.

80. Verbeek FP, van der Vorst JR, Schaafsma BE, et al. Image-guided hepatopancreatobiliary surgery using near-infrared fluorescent light. Journal of hepato-biliary-pancreatic sciences 2012:19:626-637.

81. Kudo H, Ishizawa T, Tani K, et al. Visualization of subcapsular hepatic malignancy by indocyanine-green fluorescence imaging during laparoscopic hepatectomy. Surgical endoscopy 2014:

82. Ishizawa T, Fukushima N, Shibahara J, et al. Real-time identification of liver cancers by using indocyanine green fluorescent imaging. Cancer 2009:115:2491-2504.

83. Kirschmann DA, Seftor EA, Hardy KM, et al. Molecular pathways: Vasculogenic mimicry in tumor cells: Diagnostic and therapeutic implications. Clinical cancer research : an official journal of the American Association for Cancer Research 2012:18:2726-2732.

84. Ishizawa T, Bandai Y, Ijichi M, et al. Fluorescent cholangiography illuminating the biliary tree during laparoscopic cholecystectomy. The British journal of surgery 2010:97:1369-1377.

85. Gioux S, Choi HSFrangioni JV. Image-guided surgery using invisible near-infrared light: Fundamentals of clinical translation. Molecular imaging 2010:9:237-255.

86. Chen Bde Witte PA. Photodynamic therapy efficacy and tissue distribution of hypericin in a mouse p388 lymphoma tumor model. Cancer letters 2000:150:111-117.

87. Blank M, Lavie G, Mandel M, et al. Antimetastatic activity of the photodynamic agent hypericin in the dark. International journal of cancer Journal international du cancer 2004:111:596-603.

88. Martinez-Poveda B, Quesada ARMedina MA. Hypericin in the dark inhibits key steps of angiogenesis in vitro. European journal of pharmacology 2005:516:97-103.

89. DeLaney TF, Sindelar WF, Tochner Z, et al. Phase i study of debulking surgery and photodynamic therapy for disseminated intraperitoneal tumors. International journal of radiation oncology, biology, physics 1993:25:445-457.

90. Meruelo D, Lavie GLavie D. Therapeutic agents with dramatic antiretroviral activity and little toxicity at effective doses: Aromatic polycyclic diones hypericin and pseudohypericin. Proceedings of the National Academy of Sciences of the United States of America 1988:85:5230-5234.

91. Ritz R, Daniels R, Noell S, et al. Hypericin for visualization of high grade gliomas: First clinical experience. European journal of surgical oncology : the journal of the European Society of Surgical Oncology and the British Association of Surgical Oncology 2012:38:352-360.

92. Schempp CM, Muller KA, Winghofer B, et al. [st. John's wort (hypericum perforatum l.). A plant with relevance for dermatology]. Der Hautarzt; Zeitschrift fur Dermatologie, Venerologie, und verwandte Gebiete 2002:53:316-321.

93. Keereweer S, Kerrebijn JD, van Driel PB, et al. Optical image-guided surgery--where do we stand? Molecular imaging and biology : MIB : the official publication of the Academy of Molecular Imaging 2011:13:199-207.

94. Oberlin O, Rey A, Lyden E, et al. Prognostic factors in metastatic rhabdomyosarcomas: Results of a pooled analysis from united states and european cooperative groups. Journal of clinical oncology : official journal of the American Society of Clinical Oncology 2008:26:2384-2389.

95. Laakmann G, Jahn GSchule C. [hypericum perforatum extract in treatment of mild to moderate depression. Clinical and pharmacological aspects]. Der Nervenarzt 2002:73:600-612.

96. Cheng TO. St john's wort interaction with digoxin. Archives of internal medicine 2000:160:2548.

97. Breidenbach T, Hoffmann MW, Becker T, et al. Drug interaction of st john's wort with cyclosporin. Lancet 2000:355:1912.

98. Korbelik M. Induction of tumor immunity by photodynamic therapy. Journal of clinical laser medicine & surgery 1996:14:329-334.

99. Eastin WC, Mennear JH, Tennant RW, et al. Tg.Ac genetically altered mouse: Assay working group overview of available data. Toxicologic pathology 2001:29 Suppl:60-80.

100. Fan TW, Kucia M, Jankowski K, et al. Rhabdomyosarcoma cells show an energy producing anabolic metabolic phenotype compared with primary myocytes. Molecular cancer 2008:7:79.

101. Sattler S, Schaefer U, Schneider W, et al. Binding, uptake, and transport of hypericin by caco-2 cell monolayers. Journal of pharmaceutical sciences 1997:86:1120-1126.

ACKNOWLEDGEMENTS

DECLARATION ON THE DISSERTATION

Ladies and Gentlemen,

I declare that this dissertation is the product of my own work, that it has not been submitted before for any degree or examination in any other university and that all sources I have used or quoted have been indicated and acknowledged as complete references.

Signature:

Ioan Cristian Urla